Developmental Dynamics **WILEY**

Dysregulation of Grainyhead-like 3 expression causes widespread developmental defects

Zihao Deng[1] | Tariq Butt[1] | Benedicta D. Arhatari[2,3] | Charbel Darido[4,5] | Alana Auden[1] | Dijina Swaroop[1] | Darren D. Partridge[1] | Katharina Haigh[6,7] | Thao Nguyen[8] | Jody J. Haigh[6,7] | Marina R. Carpinelli[1] | Stephen M. Jane[1]

[1]Department of Medicine (Alfred Hospital), Central Clinical School, Monash University, Melbourne, Victoria, Australia

[2]ARC Centre of Excellence in Advanced Molecular Imaging, Department of Chemistry and Physics, La Trobe University, Bundoora, Victoria, Australia

[3]Australian Synchrotron, ANSTO, Clayton, Victoria, Australia

[4]Peter MacCallum Cancer Centre, Melbourne, Victoria, Australia

[5]Sir Peter MacCallum Department of Oncology, The University of Melbourne, Parkville, Victoria, Australia

[6]Department of Pharmacology and Therapeutics, Rady Faculty of Health Sciences, University of Manitoba, Winnipeg, Manitoba, Canada

[7]Research Institute in Oncology and Hematology, CancerCare Manitoba, Winnipeg, Manitoba, Canada

[8]Australian Centre for Blood Diseases, Central Clinical School, Monash University, Melbourne, Victoria, Australia

Correspondence
Stephen M. Jane, Department of Medicine (Alfred Hospital), Central Clinical School, Monash University, 99 Commercial Rd, Melbourne, VIC, 3004, Australia.
Email: stephen.jane@monash.edu

Abstract

Background: The gene encoding the transcription factor, Grainyhead-like 3 (*Grhl3*), plays critical roles in mammalian development and homeostasis. *Grhl3*-null embryos exhibit thoraco-lumbo-sacral spina bifida and soft-tissue syndactyly. Additional studies reveal that these embryos also exhibit an epidermal proliferation/differentiation imbalance. This manifests as skin barrier defects resulting in peri-natal lethality and defective wound repair. Despite these extensive analyses of *Grhl3* loss-of-function models, the consequences of gain-of-function of this gene have been difficult to achieve.

Results: In this study, we generated a novel mouse model that expresses *Grhl3* from a transgene integrated in the *Rosa26* locus on an endogenous *Grhl3*-null background. Expression of the transgene rescues both the neurulation and skin barrier defects of the knockout mice, allowing survival into adulthood. Despite this, the mice are not normal, exhibiting a range of phenotypes attributable to dysregulated *Grhl3* expression. In mice homozygous for the transgene, we observe a severe Shaker-Waltzer phenotype associated with hearing impairment. Micro-CT scanning of the inner ear revealed profound structural alterations underlying these phenotypes. In addition, these mice exhibit other developmental anomalies including hair loss, digit defects, and epidermal dysmorphogenesis.

Conclusion: Taken together, these findings indicate that diverse developmental processes display low tolerance to dysregulation of *Grhl3*.

KEYWORDS
Grhl3 overexpression, inner ear malformation, neural tube defects, Shaker-Waltzer phenotype, skin barrier defects

1 | INTRODUCTION

Grainyhead-like 3 (*Grhl3*), is a member of a family of mammalian transcription factors descended from the *Drosophila* grainyhead (*grh*) gene.[1-3] During murine embryogenesis, *Grhl3* is predominantly expressed in the surface ectoderm from embryonic day (E) 8.5.[4] Expression is also observed along the E8.5 neural plate border from which the otic placode arises from the pre-placodal region and in the inner and outer hair cell of the cochlea.[4-7] *Grhl3* plays critical roles in mammalian development and homeostasis that have been uncovered through analysis of loss-of-function models. Constitutive gene inactivation in embryogenesis leads to a failure of caudal neural tube closure, which manifests as thoraco-lumbo-sacral spina bifida—a major subtype of neural tube defects (NTDs), and a hypomorphic *Grhl3* allele has been identified as the underlying defect in the curly tail (*ct*) mouse strain, a model of neural tube closure for more than 50 years.[8,9] The abnormal neural tube morphogenesis observed in *Grhl3-null* animals has been recently shown to correlate with altered and disorganized cellular protrusions in the surface ectoderm, which presumably compromises the zippering of neural tube along the spinal axis.[10] *Grhl3*-null embryos also exhibit soft-tissue syndactyly, and a shortened anterior-posterior axis due to defects in the planar cell polarity signaling pathway.[5,11,12] The latter also manifests as defective wound healing and perturbed stereociliary bundles in the inner ear.[5,11] Newborn *Grhl3*-null mice die soon after birth of dehydration due to a failure of the skin barrier to form and exhibit a marked disruption in keratinocyte differentiation and impaired epidermal architecture.[11,13-16] In the adult, conditional inactivation of *Grhl3* in the squamous epithelial tissues of the skin and head and neck reproduces this proliferation/differentiation imbalance and leads to squamous cell carcinoma, establishing *Grhl3* as a critical tumor suppressor at these sites.[15,17] In humans, mutations in *GRHL3* are associated with Van der Woude syndrome that is characterized by cleft palate and are recognized as a major predisposing factor for spina bifida.[18-20] Multiple de novo and inherited variants have been reported in patients with NTDs.[19,20]

To date, only one mouse overexpression model utilizing a bacterial artificial chromosome (BAC)-containing *Grhl3* has been reported.[21] In this study, ∼1.5 to 2-fold overexpression of *Grhl3* was associated with spina bifida.[21] In zebrafish, overexpression of *Grhl3* through microinjection of full-length *Grhl3* mRNA into the 1-2 cell stage embryos yielded axial defects but not NTDs.[22] In the current study, we established and characterized a novel mouse model of *Grhl3* misexpression. In contrast to the previous study,[21] we did not identify NTDs in transgenic mice with *Grhl3* overexpression but identified multiple other developmental defects, emphasizing the need for stringent regulation of this gene during murine embryogenesis.

2 | RESULTS

2.1 | Restoration of *Grhl3* expression in *Grhl3*-knockout mice rescues skin barrier and neural tube defects

We and others have previously attempted to generate mouse lines overexpressing *Grhl3* using a wide variety of regulatory elements to drive expression, including the keratin (*K*)-14, *CAG*, and B6 (*CMV*) promoters (Kimura-Yoshida et al[23] and unpublished data). Despite multiple rounds of injections, we never identified any pups expressing the transgene, suggesting that overexpression of *Grhl3* is incompatible with embryonic survival. This was subsequently affirmed, with *Grhl3* transgenic embryos shown to undergo growth arrest and death at E5.5.[23] To redress this, we devised a strategy to express a *Flag-Grhl3* transgene on a *Grhl3*-null background. The transgene was inserted into the murine *Rosa26* locus, allowing expression of *Flag-Grhl3* from the *Rosa26* regulatory elements ($Rosa26^{Grhl3\ cDNA}$, Figure 1A).[24] Tissue- and temporal-specificity was achieved through deletion of a *loxP-STOP-loxP* cassette in the *Rosa26* locus immediately upstream of the *Flag-Grhl3* coding region that was induced by an intercross of the $Rosa26^{Grhl3\ cDNA/Grhl3\ cDNA}$ line with a line in which the *Cre* recombinase gene had been knocked into the endogenous *Grhl3* locus, rendering *Cre*-positive mice *Grhl3*-heterozygotes (Figure 1B,C).[25] Further crosses generated offspring that were null at the endogenous locus ($Grhl3^{Cre/Cre}$) and heterozygous or homozygous for the transgene (Figure 1C–E). Intact transgene knock-in was confirmed by Sanger DNA sequencing, and deletion of the *loxP-STOP-loxP* cassette was confirmed by PCR analysis (Figure 1F). Dissection of uteri from $Grhl3^{Cre/+}$;$Rosa26^{Grhl3\ cDNA/+}$ intercrosses at both E14.5 and E18.5 frequently showed litters of three to four embryos (expected litter size average 6.5 embryos[26]), with a high number of resorptions. Genotyping of 42 offspring at E14.5 and 323 offspring at E18.5 showed that wild-type embryos (WT—$Grhl3^{+/+}$;$Rosa26^{+/+}$), embryos heterozygous for the *Grhl3-Cre* allele or the transgene or both ($Grhl3^{Cre/+}$;$Rosa26^{+/+}$, $Grhl3^{+/+}$;$Rosa26^{Grhl3\ cDNA/+}$, $Grhl3^{Cre/+}$;$Rosa26^{Grhl3\ cDNA/+}$), and embryos homozygous for the *Grhl3-Cre* allele ($Grhl3^{Cre/Cre}$;$Rosa26^{Grhl3\ cDNA/+}$, $Grhl3^{Cre/Cre}$;$Rosa26^{+/+}$) were present at the predicted Mendelian ratios, whereas under-representation of embryos carrying two alleles of the *Grhl3* transgene
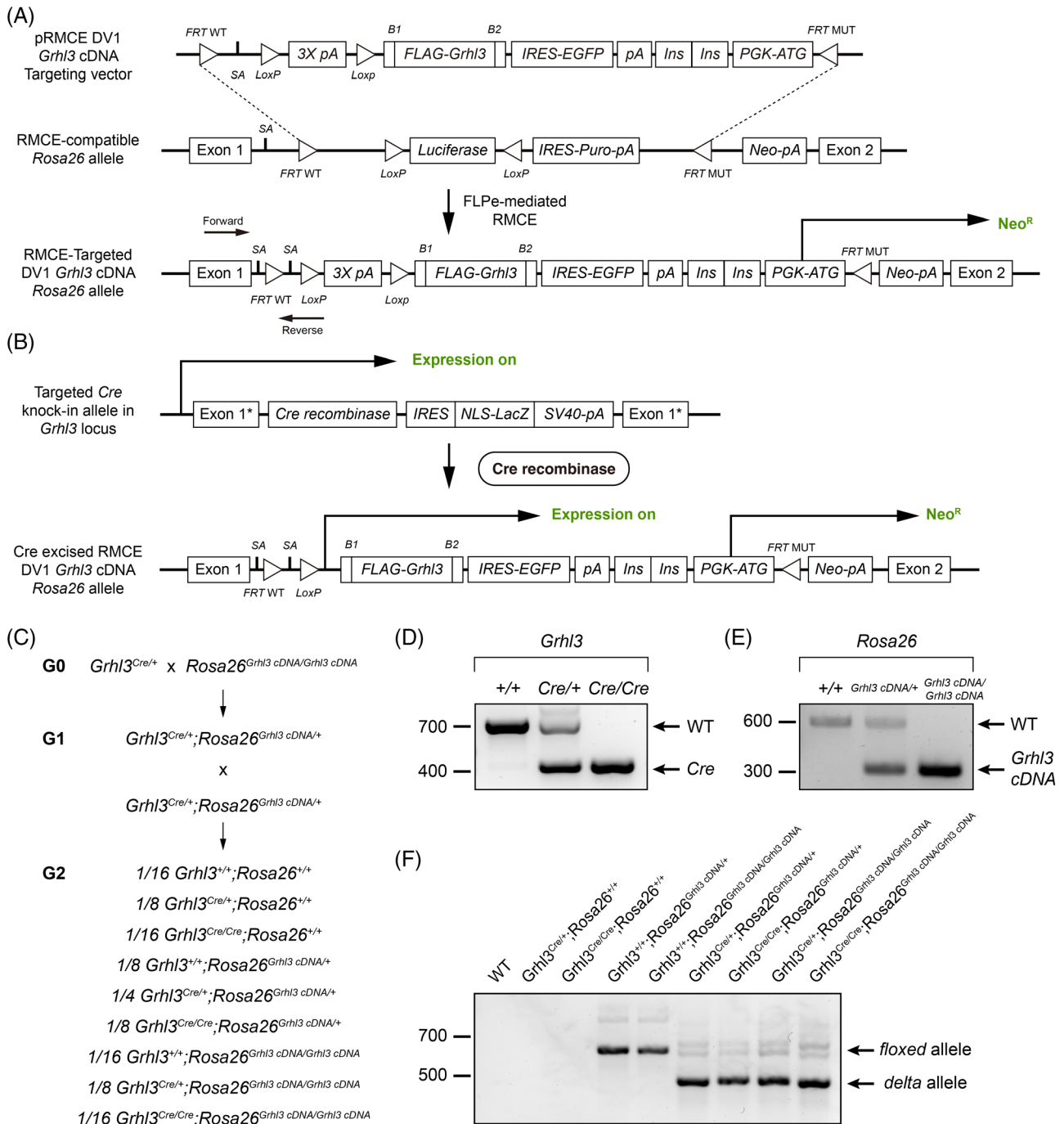
FIGURE 1 Generation of *Grhl3*^*Cre*^;*Rosa26*^*Grhl3 cDNA*^ transgenic mouse model. (A) Gene-targeting strategy for making *Rosa26*^*Grhl3 cDNA*^ allele. The *loxP-STOP-loxP-Flag-Grhl3* transgene was targeted into the RMCE-compatible *Rosa26* locus of murine G4 ROSALUC embryonic stem cells. (B) With the presence of the Cre recombinase, the expression of the transgene will be constantly activated, which is driven by the *Rosa26* promoter, after the Cre-mediated excision of the *loxP*-flanked transcriptional stop sequence (*loxP-STOP-loxP*). (C) G1 *Grhl3*^*Cre/+*^;*Rosa26*^*Grhl3 cDNA/+*^ mice is generated by crossing G0 breeding pairs, *Grhl3*^*Cre/+*^ and *Rosa26*^*Grhl3 cDNA/Grhl3 cDNA*^ mice. Intercrossing of G1 *Grhl3*^*Cre/+*^;*Rosa26*^*Grhl3 cDNA/+*^ mice generated offspring with nine different genotypes. (D) PCR genotyping of *Grhl3*^*Cre*^ allele. WT, product of wild-type *Grhl3* allele; *Cre*, product of targeted *Grhl3* allele. (E) PCR genotyping of *Rosa26*^*Grhl3 cDNA*^ allele. WT, product of wild-type *Rosa26* allele; *Tg*, product of targeted *Rosa26* allele. (F) Representative PCR products of *floxed* allele and *delta* allele of *Grhl3* transgene on *Rosa26* locus

(*Grhl3*^*+/+*^;*Rosa26*^*Grhl3 cDNA/Grhl3 cDNA*^, *Grhl3*^*Cre/+*^; *Rosa26*^*Grhl3 cDNA/Grhl3 cDNA*^ and *Grhl3*^*Cre/Cre*^;*Rosa26*^*Grhl3 cDNA/Grhl3 cDNA*^) was observed (Table 1). Surprisingly, this

under-representation was not dependent on the presence of a *Cre* allele. Genotyping of 104 observed resorptions with only minimal residual embryonic tissues at E18.5

TABLE 1 Expected and observed numbers of embryos carrying corresponding genotypes from the intercross of $Grhl3^{Cre/+}$;$Rosa26^{Grhl3\ cDNA/+}$ mice at E14.5 and E18.5

Genotype	Expected number of embryos	Observed number of embryos	P value
a. E14.5			
$Grhl3^{+/+}$;$Rosa26^{+/+}$	4.0625	2	.31
$Grhl3^{Cre/+}$;$Rosa26^{+/+}$	8.125	6	.46
$Grhl3^{Cre/Cre}$;$Rosa26^{+/+}$	4.0625	4	.98
$Grhl3^{+/+}$;$Rosa26^{Grhl3\ cDNA/+}$	8.125	8	.97
$Grhl3^{Cre/+}$;$Rosa26^{Grhl3\ cDNA/+}$	16.25	15	.76
$Grhl3^{Cre/Cre}$;$Rosa26^{Grhl3\ cDNA/+}$	8.125	7	.69
$Grhl3^{+/+}$;$Rosa26^{Grhl3\ cDNA/Grhl3\ cDNA}$	4.0625	0	**.04***
$Grhl3^{Cre/+}$;$Rosa26^{Grhl3\ cDNA/Grhl3\ cDNA}$	8.125	0	**.004***
$Grhl3^{Cre/Cre}$;$Rosa26^{Grhl3\ cDNA/Grhl3\ cDNA}$	4.0625	0	**.04***
Total number from 10 litters	65	42	**.004***
b. E18.5			
$Grhl3^{+/+}$;$Rosa26^{+/+}$	26	32	.24
$Grhl3^{Cre/+}$;$Rosa26^{+/+}$	52	51	.89
$Grhl3^{Cre/Cre}$;$Rosa26^{+/+}$	26	24	.69
$Grhl3^{+/+}$;$Rosa26^{Grhl3\ cDNA/+}$	52	57	.49
$Grhl3^{Cre/+}$;$Rosa26^{Grhl3\ cDNA/+}$	104	89	.14
$Grhl3^{Cre/Cre}$;$Rosa26^{Grhl3\ cDNA/+}$	52	43	.21
$Grhl3^{+/+}$;$Rosa26^{Grhl3\ cDNA/Grhl3\ cDNA}$	26	5	**.00004***
$Grhl3^{Cre/+}$;$Rosa26^{Grhl3\ cDNA/Grhl3\ cDNA}$	52	12	**<.00001***
$Grhl3^{Cre/Cre}$;$Rosa26^{Grhl3\ cDNA/Grhl3\ cDNA}$	26	10	**.0017***
Total number from 64 litters	416	323	**<.00001***

Note: Expected numbers of embryos were calculated as average litter size of 6.5 embryos. A one sample χ^2 test was used for data analysis. P values are for comparison between the expected and observed number of embryos.

*P value <.05.

from 26 litters showed that 73 of which were $Grhl3^{Cre/+}$;$Rosa26^{Grhl3\ cDNA/+}$, 15 were $Grhl3^{Cre/Cre}$;$Rosa26^{Grhl3\ cDNA/+}$, 5 were $Grhl3^{Cre/Cre}$;$Rosa26^{Grhl3\ cDNA/+}$ and 11 were $Grhl3^{Cre/Cre}$;$Rosa26^{Grhl3\ cDNA/Grhl3\ cDNA}$. No resorbed embryo was genotyped as $Grhl3^{+/+}$;$Rosa26^{Grhl3\ cDNA/Grhl3\ cDNA}$.

To assess the level of $Grhl3$ expression, we isolated epidermis from E18.5 embryos and performed quantitative reverse transcription PCR (Q-RT-PCR) analyses using primer pairs that would selectively amplify endogenous $Grhl3$, transgene-derived $Grhl3$, or both. As expected, no endogenous $Grhl3$ mRNA was detected in any embryos genotyped as $Grhl3^{Cre/Cre}$, and no transgene expression was seen in $Rosa26^{+/+}$ embryos (Figure 2A–C). Importantly, no leaky $Grhl3$ transgene expression was detected in survived E18.5 $Grhl3^{+/+}$; $Rosa26^{Grhl3\ cDNA/Grhl3\ cDNA}$ embryos (Figure 2C). Embryos heterozygous for both endogenous $Grhl3$ and the transgene ($Grhl3^{Cre/+}$;$Rosa26^{Grhl3\ cDNA/+}$), and embryos carrying a single copy of the transgene in the absence of endogenous $Grhl3$ ($Grhl3^{Cre/Cre}$;$Rosa26^{Grhl3\ cDNA/+}$), had expression levels equivalent to WT embryos (Figure 2A). Embryos homozygous for the transgene and homozygous or heterozygous for endogenous $Grhl3$ ($Grhl3^{Cre/+}$; $Rosa26^{Grhl3\ cDNA/Grhl3\ cDNA}$ and $Grhl3^{Cre/Cre}$;$Rosa26^{Grhl3\ cDNA/Grhl3\ cDNA}$) exhibited an approximately 2-2.5-fold increase in total $Grhl3$ mRNA levels compared to WT (Figure 2A). Attempt at quantitation of GRHL3 protein level in E18.5 epidermis by immunoblotting with an anti-GRHL3 antibody was unsuccessful (Figure 2D) given the presence of signal in constitutive $Grhl3$-null samples. However, the expression of the reporter for transgene expression, GFP, was only detected in embryos carrying both $Grhl3$-Cre and transgene (Figure 2D).

As identified in our previous studies,[11] inactivation of both endogenous $Grhl3$ alleles (as seen in $Grhl3^{Cre/Cre}$;
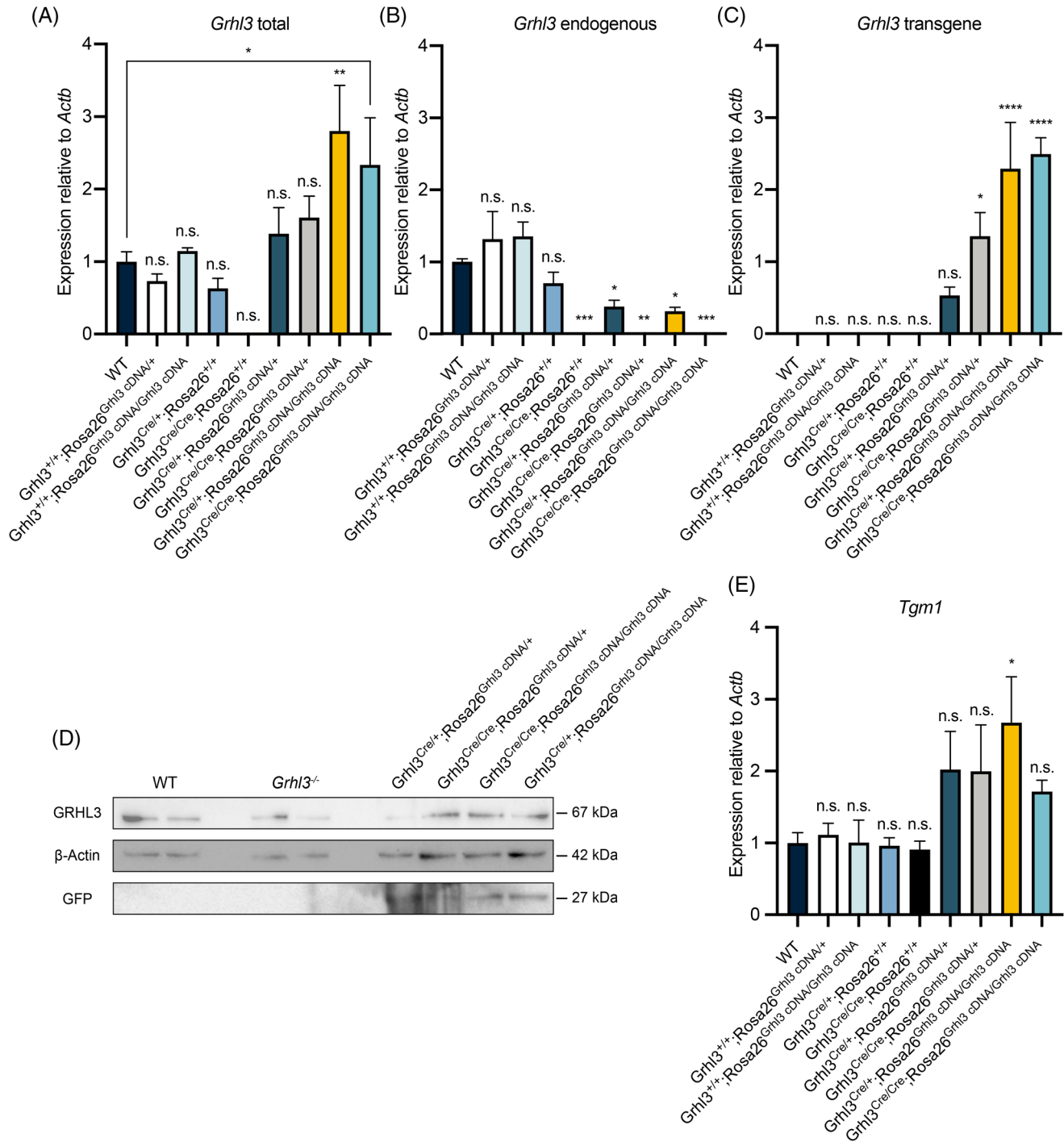
FIGURE 2 Misexpression of *Grhl3* in *Grhl3^Cre*;*Rosa26^Grhl3 cDNA* transgenic mouse model. Q-RT-PCR on E18.5 epidermis showing abundance of total *Grhl3* mRNA (A), endogenous *Grhl3* mRNA (B) and transgene *Grhl3* mRNA (C) varies across genotypes. (D) Western blot analysis of GRHL3 and GFP protein expression in E18.5 wild-type, constitutive *Grhl3*-null and transgenic mice. (E) Q-RT-PCR on E18.5 epidermis showing comparable expression levels of *Tgm1* in wild-type and transgenic mice. Bar graph presented as a mean ± standard error of mean (SEM). A one-way ANOVA test following by a Dunnett's multiple comparison test between wild-type and other genotypes were used for data analysis. An additional Mann-Whitney test was used to compare the total *Grhl3* mRNA level (A) between E18.5 wild-type and *Grhl3^Cre/Cre*;*Rosa26^Grhl3 cDNA/Grhl3 cDNA* epidermis. *P value <.05, **P-value <.01, ***P value <.001, ****P value <.00001. n.s., not significant

Rosa26^+/+ embryos) leads to a profound skin barrier defect, as evidenced by penetration of the externally delivered dye, toluidine blue (Figure 3B),[27] with WT

embryos excluding the dye (Figure 3A). The *Grhl3^Cre/Cre*; *Rosa26^+/+* embryos further mimicked the *Grhl3^−/−* mice, displaying fully penetrant thoraco-lumbo-sacral spina
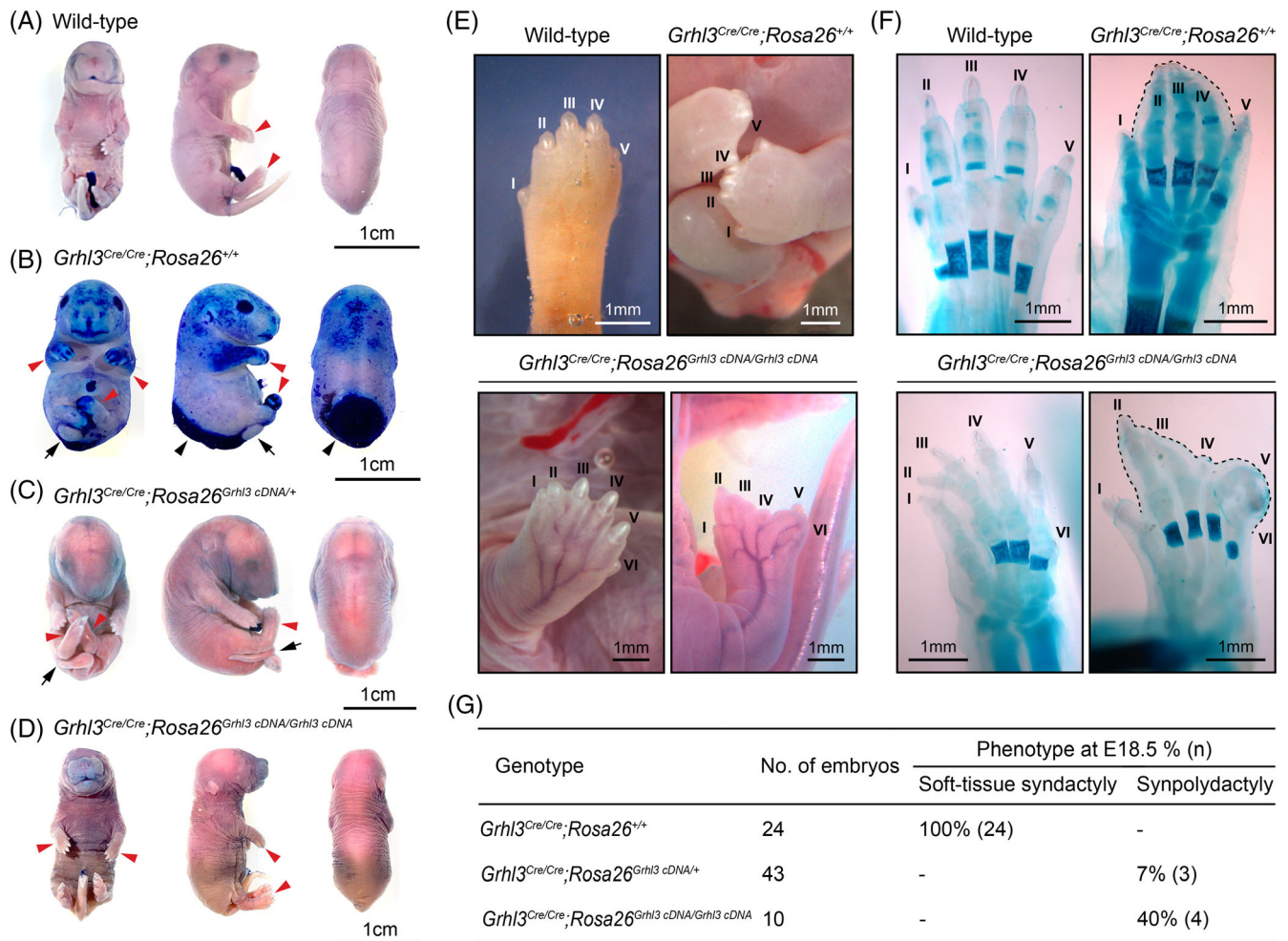
FIGURE 3 Restoration of *Grhl3* expression rescues neurulation and skin barrier defects of *Grhl3*-null mice while misexpression of *Grhl3* expression causes digit defects. (A-D) Skin barrier assay on E18.5 wild-type and transgenic mice. Wild-type embryos (N = 4) showed a fully acquired skin barrier (A). Penetration of toluidine blue into skin indicated impaired skin barrier in *Grhl3*$^{Cre/Cre}$;*Rosa26*$^{+/+}$ embryos (N = 4). *Grhl3*$^{Cre/Cre}$;*Rosa26*$^{+/+}$ embryos also showed syndactyly, curly tail and spina bifida (B). Restoration of *Grhl3* expression rescued skin barrier defect and spina bifida in *Grhl3*$^{Cre/Cre}$;*Rosa26*$^{Grhl3\ cDNA/+}$ embryos (N = 4) (C). Over-expression of *Grhl3* in *Grhl3*$^{Cre/Cre}$;*Rosa26*$^{Grhl3\ cDNA/Grhl3\ cDNA}$ embryos (N = 4) fully rescued *Ghrl3*-null phenotypes (D). (E) Gross appearance of digits from wild-type (N = 4), *Grhl3*$^{Cre/Cre}$;*Rosa26*$^{+/+}$ (N = 4) and *Grhl3*$^{Cre/Cre}$;*Rosa26*$^{Grhl3\ cDNA/Grhl3\ cDNA}$ (N = 4) embryos at E18.5. (F) Skeletal preparations of wild-type (N = 4), *Grhl3*$^{Cre/Cre}$; *Rosa26*$^{+/+}$ (N = 4) and *Grhl3*$^{Cre/Cre}$;*Rosa26*$^{Grhl3\ cDNA/Grhl3\ cDNA}$ (N = 2) embryos at E18.5. *Grhl3*$^{Cre/Cre}$;*Rosa26*$^{+/+}$ embryos exhibited soft-tissue syndactyly. *Grhl3*$^{Cre/Cre}$;*Rosa26*$^{Grhl3\ cDNA/Grhl3\ cDNA}$ embryos exhibited synpolydactyly and incompletely formed digits. The dotted line outlines the soft-tissue syndactyly. (G) Penetrance of digit defects among *Grhl3*$^{Cre/Cre}$;*Rosa26*$^{+/+}$, *Grhl3*$^{Cre/Cre}$;*Rosa26*$^{Grhl3\ cDNA/+}$ and *Grhl3*$^{Cre/Cre}$;*Rosa26*$^{Grhl3\ cDNA/Grhl3\ cDNA}$ embryos at E18.5. Arrows, curly tail; black arrowheads, spina bifida; red arrowheads, digits

bifida, curly tail, open eyelids, round body shape and a short longitudinal embryonic axis (Figure 3B). *Grhl3*$^{Cre/Cre}$;*Rosa26*$^{+/+}$ embryos also showed oedematous limbs, with soft-tissue syndactyly (Figure 3E–G), and died soon after birth, phenocopying the *Grhl3*$^{-/-}$ embryos.[11,12,21] Rescue of the skin barrier defect was observed in *Grhl3*$^{Cre/Cre}$;*Rosa26*$^{Grhl3\ cDNA/+}$ embryos, indicative of functional GRHL3 protein derived from the transgene in these animals (Figure 3C). Spina bifida was also rescued in these mice, although a shortened longitudinal axis and residual

curly tail was observed, suggesting that functional GRHL3 protein levels in this context were approximately 30% of WT (and similar to the *curly tail* strain). NTDs were fully rescued in mice carrying two copies of the transgene (*Grhl3*$^{Cre/Cre}$;*Rosa26*$^{Grhl3\ cDNA/Grhl3\ cDNA}$), as was the skin barrier defect (Figure 3D), indicating that overexpression of *Grhl3* is compatible with normal neural tube closure and epidermal barrier function. One novel developmental consequence of *Grhl3* overexpression was observed, with 40% of the *Grhl3*$^{Cre/Cre}$;*Rosa26*$^{Grhl3\ cDNA/Grhl3\ cDNA}$ embryos

displaying synpolydactyly, with incomplete digit formation, indicating impaired digit patterning and morphogenesis (Figure 3E–G). This was also observed with lower penetrance in the $Grhl3^{Cre/Cre}$;$Rosa26^{Grhl3\ cDNA/+}$ embryos (7%), suggesting a dose response (Figure 3G).

2.2 | Restoration of *Grhl3* expression in *Grhl3*-knockout mice partially rescues epidermal differentiation

We next examined the epidermal architecture in the various mouse lines at E18.5 using hematoxylin and eosin (H&E) staining and immunohistochemistry (IHC) analysis with proliferative and cell differentiation markers. Consistent with our previous findings in *Grhl3*-null embryos,[11,15] $Grhl3^{Cre/Cre}$;$Rosa26^{+/+}$ embryos displayed a markedly thicker epidermis compared with WT embryos (Figure 4). In addition, the stratum corneum (SC) layer of $Grhl3^{Cre/Cre}$;$Rosa26^{+/+}$ epidermis was compacted, and both the stratum granulosum (SG) and stratum spinosum (SP) layers were expanded. Interestingly, we noticed an extra tissue structure residing superiorly to the SC of $Grhl3^{Cre/Cre}$;$Rosa26^{+/+}$ epidermis. This structure contained an underlying anucleate layer, attached to the SC, and a superior layer of nucleated cells (Figure 4). Kashgari et al[12] have recently identified that GRHL3 is necessary for periderm morphogenesis and nonadhesive function as digits separate. We postulate that this extra tissue structure may result from periderm dysmorphogenesis due to inactivation of *Grhl3*. Despite its normal barrier function, the epidermal architecture of $Grhl3^{Cre/Cre}$;$Rosa26^{Grhl3\ cDNA/+}$ embryos reassembled that of $Grhl3^{Cre/Cre}$;$Rosa26^{+/+}$ epidermis but without the extra tissue structure (Figure 4). $Grhl3^{Cre/+}$;$Rosa26^{Grhl3\ cDNA/+}$, $Grhl3^{Cre/+}$;$Rosa26^{Grhl3\ cDNA/Grhl3\ cDNA}$ and $Grhl3^{Cre/Cre}$;$Rosa26^{Grhl3\ cDNA/Grhl3\ cDNA}$ epidermis exhibited a normal morphological appearance (Figure 4).

IHC analysis of various cell differentiation markers on E18.5 epidermis showed that the expression domain of the basal marker, K5, was expanded into layers above the SB of the $Grhl3^{Cre/Cre}$;$Rosa26^{+/+}$ epidermis. K5 expression in $Grhl3^{Cre/Cre}$;$Rosa26^{Grhl3\ cDNA/+}$, $Grhl3^{Cre/+}$;$Rosa26^{Grhl3\ cDNA/+}$, $Grhl3^{Cre/+}$;$Rosa26^{Grhl3\ cDNA/Grhl3\ cDNA}$ and $Grhl3^{Cre/Cre}$;$Rosa26^{Grhl3\ cDNA/Grhl3\ cDNA}$ epidermis resembled the WT control (Figure 4). Similar normalization of expression was seen with the terminal differentiation markers loricrin and filaggrin, and the suprabasal marker K1 in $Grhl3^{Cre/Cre}$;$Rosa26^{Grhl3\ cDNA/+}$, $Grhl3^{Cre/+}$;$Rosa26^{Grhl3\ cDNA/+}$, $Grhl3^{Cre/+}$;$Rosa26^{Grhl3\ cDNA/Grhl3\ cDNA}$ and $Grhl3^{Cre/Cre}$;$Rosa26^{Grhl3\ cDNA/Grhl3\ cDNA}$ embryos compared with the $Grhl3^{Cre/Cre}$;$Rosa26^{+/+}$ epidermis, indicating that restoration of *Grhl3* expression largely redressed

the differentiation defects that are the hallmark of *Grhl3*-null epidermis. Positive staining with all four of these markers was observed in the extra tissue layer above the SC in the $Grhl3^{Cre/Cre}$;$Rosa26^{+/+}$ epidermis. This observation suggests that the extra tissue layer contained differentiating cells. Only K6, a marker of epidermal repair, was mildly upregulated in the $Grhl3^{Cre/Cre}$;$Rosa26^{Grhl3\ cDNA/+}$ and $Grhl3^{Cre/+}$;$Rosa26^{Grhl3\ cDNA/+}$ epidermis compared to WT (Figure 4), but expression of this marker was markedly lower than in $Grhl3^{Cre/Cre}$;$Rosa26^{+/+}$ epidermis. Consistent with normalization of differentiation markers and barrier function in embryos expressing endogenous or transgene-derived GRHL3, Transglutaminase 1 (*Tgm1*), a direct GRHL3 target gene critical for epidermal barrier formation,[11,28] was expressed in epidermis from the $Grhl3^{Cre/+}$;$Rosa26^{Grhl3\ cDNA/Grhl3\ cDNA}$, $Grhl3^{Cre/+}$;$Rosa26^{Grhl3\ cDNA/+}$, $Grhl3^{Cre/Cre}$;$Rosa26^{Grhl3\ cDNA/+}$, and $Grhl3^{Cre/Cre}$;$Rosa26^{Grhl3\ cDNA/Grhl3\ cDNA}$ embryos (Figure 2E).

We then examined the expression of two proliferation marker, PCNA and Ki67, in E18.5 transgenic epidermis. PCNA-positive cells were widely distributed in both basal and suprabasal layers with disorganized cellular arrangement in the $Grhl3^{Cre/Cre}$;$Rosa26^{+/+}$ and $Grhl3^{Cre/Cre}$;$Rosa26^{Grhl3\ cDNA/Grhl3\ cDNA}$ epidermis with more than 80% of epidermal cells being PCNA-positive in the latter, indicating keratinocyte hyperproliferation (Figure 5A,B). The $Grhl3^{Cre/Cre}$;$Rosa26^{Grhl3\ cDNA/+}$ and $Grhl3^{Cre/+}$;$Rosa26^{Grhl3\ cDNA/Grhl3\ cDNA}$ epidermis also showed significantly higher percentage of PCNA-positive cells compared to WT (Figure 5A,B). In contrast, PCNA positivity in the $Grhl3^{Cre/+}$;$Rosa26^{Grhl3\ cDNA/+}$ epidermis did not differ from the WT control (Figure 5A,B). The similar pattern was also observed in Ki67 IHC analysis, with more than 60% of Ki67-positive cells presented in the $Grhl3^{Cre/Cre}$;$Rosa26^{Grhl3\ cDNA/Grhl3\ cDNA}$ epidermis and a significantly increased Ki67 positivity in the $Grhl3^{Cre/Cre}$;$Rosa26^{+/+}$, $Grhl3^{Cre/Cre}$;$Rosa26^{Grhl3\ cDNA/+}$ and $Grhl3^{Cre/+}$;$Rosa26^{Grhl3\ cDNA/Grhl3\ cDNA}$ epidermis compared to that of WT control, confirming the observed basal hyperproliferation in the PCNA IHC analysis.

2.3 | Overexpression of *Grhl3* perturbs epidermal homeostasis in adult mice

To explore the consequences of *Grhl3* overexpression, we followed the progress of aging $Grhl3^{Cre/+}$;$Rosa26^{Grhl3\ cDNA/Grhl3\ cDNA}$ and $Grhl3^{Cre/Cre}$;$Rosa26^{Grhl3\ cDNA/Grhl3\ cDNA}$ mice, which we had shown previously were the two genotypes with excess total *Grhl3* expression compared to WT mice (Figure 1A). We observed severe alopecia in the dorsal region and tails of mice of both genotypes
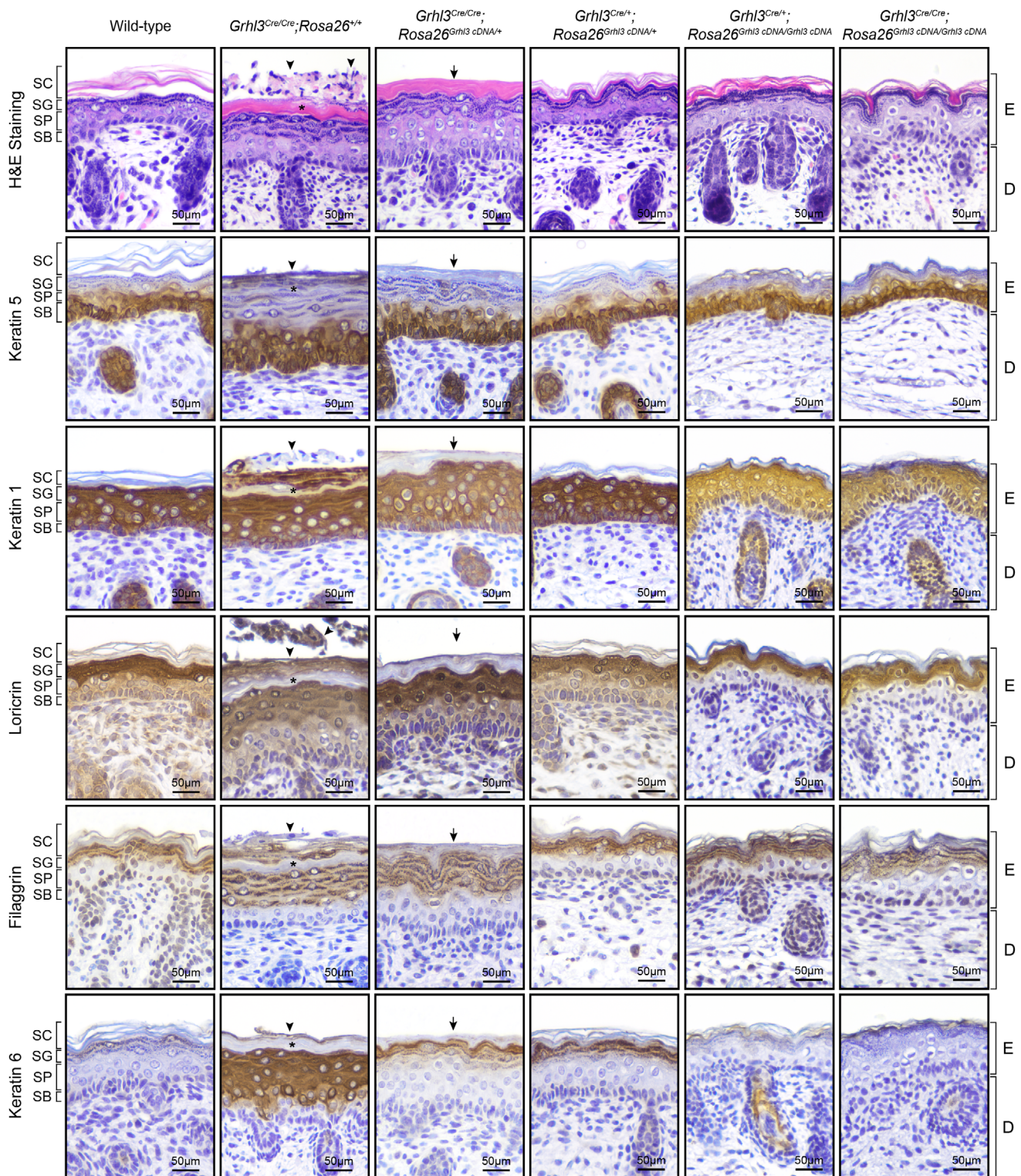
FIGURE 4 Restoration of *Grhl3* expression partially rescues epidermis abnormalities in embryos. Histological and immunostaining analysis of wild-type and transgenic E18.5 epidermis. N = 4. Arrowheads, the extra tissue structure residing superiorly to the epidermis; asterisks, compacted stratum corneum layer between the extra tissue structure and the stratum granulosum layer; arrows, compacted stratum corneum layer. SC, stratum corneum; SG, stratum granulosum; SP, stratum spinosum; SB, stratum basale; E, epidermis; D, dermis

(Figure 6A). H&E staining of hair follicles showed evident clefts between the inner root sheath (IRS) and the outer root sheath (ORS) of the *Grhl3^Cre/+^;Rosa26^Grhl3 cDNA/Grhl3 cDNA^* and *Grhl3^Cre/Cre^;Rosa26^Grhl3 cDNA/Grhl3 cDNA^* adult mice but not in age-matched WT controls (Figure 6B). This finding was reminiscent of the *Grhl1-*
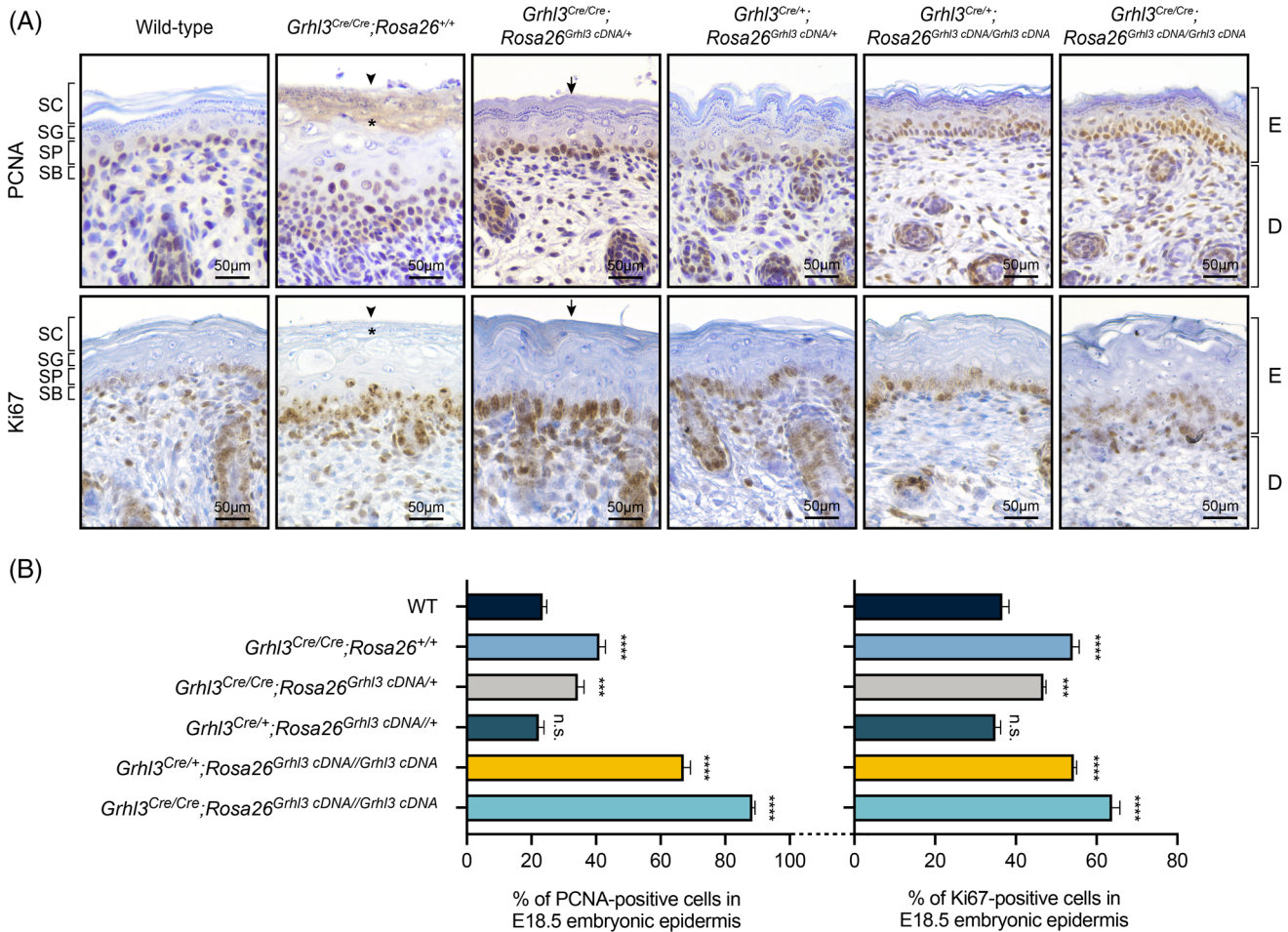
FIGURE 5 Misexpression of *Grhl3* expression leads to basal keratinocyte hyperproliferation. PCNA and Ki67 immunostaining analyses and quantifications of PCNA- and Ki67-positive cells in wild-type and transgenic E18.5 epidermis. N = 4. Arrowheads, the extra tissue structure residing superiorly to the epidermis; asterisks, compacted stratum corneum layer between the extra tissue structure and the stratum granulosum layer; arrows, compacted stratum corneum layer. SC, stratum corneum; SG, stratum granulosum; SP, stratum spinosum; SB, stratum basale; E, epidermis; D, dermis. Bar graph presented as a mean $\pm$ standard error of mean (SEM). A one-way ANOVA test following by a Dunnett's multiple comparison test between wild-type and other genotypes were used for data analysis. ***P value <.001, ****P value <.00001. n.s., not significant

knockout adult mice, which exhibit regional hair loss with grooming, due to loss of expression of its direct target gene Desmoglein-1a (*Dsg1a*), a desmosome component important for hair shaft anchorage.[29] Q-RT-PCR analysis of the epidermis showed comparable levels of *Grhl1* and *Dsg1a* expression in *Grhl3*^Cre/+^;*Rosa26*^Grhl3 cDNA/Grhl3 cDNA^ and *Grhl3*^Cre/Cre^;*Rosa26*^Grhl3 cDNA/Grhl3 cDNA^ mice and WT controls (Figure 7A,B), suggesting that alternate mechanisms underlie alopecia mediated by *Grhl3* overexpression.

H&E staining showed no difference in epidermal architecture between WT, *Grhl3*^Cre/+^;*Rosa26*^Grhl3 cDNA/Grhl3 cDNA^ and *Grhl3*^Cre/Cre^;*Rosa26*^Grhl3 cDNA/Grhl3 cDNA^ adult epidermis (Figure 6C). Expression patterns of K5, K14, loricrin and involucrin were also comparable between WT, *Grhl3*^Cre/+^;*Rosa26*^Grhl3 cDNA/Grhl3 cDNA^ and

Grhl3^Cre/Cre^;*Rosa26*^Grhl3 cDNA/Grhl3 cDNA^ epidermis (Figure 6C). However, there was a very subtle elevation of K6 expression in the adult *Grhl3*^Cre/+^;*Rosa26*^Grhl3 cDNA/Grhl3 cDNA^ and *Grhl3*^Cre/Cre^;*Rosa26*^Grhl3 cDNA/Grhl3 cDNA^ epidermis, whereas no K6 expression was detected in WT adult epidermis (Figure 6C). These findings indicate that normal *Grhl3* expression in the epidermis is also necessary for epidermal hemostasis during postnatal life.

Examination of PCNA and Ki67 expression revealed a well-organized lining of PCNA- and Ki67-cells, largely confined to the SB layer of WT epidermis. In contrast, PCNA and Ki67 expression in both the *Grhl3*^Cre/+^; *Rosa26*^Grhl3 cDNA/Grhl3 cDNA^, and the *Grhl3*^Cre/Cre^; *Rosa26*^Grhl3 cDNA/Grhl3 cDNA^ epidermis was not confined to the basal layer, with PCNA- and Ki67-positive cells visible in the suprabasal regions, and highly disorganized in
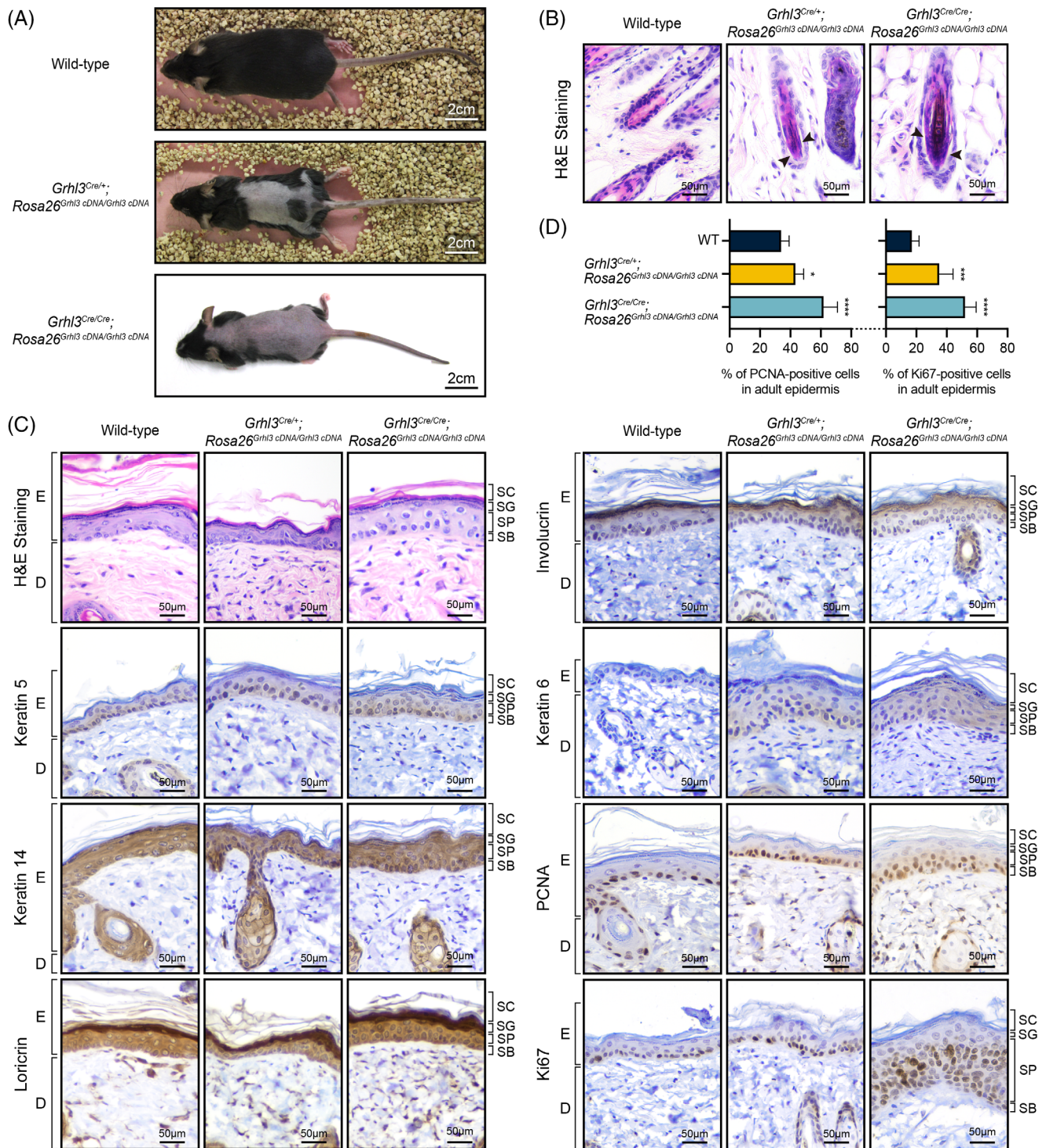
FIGURE 6 Overexpression of *Grhl3* perturbs epidermal homeostasis in adult. (A) Adult *Grhl3*^{Cre/+};*Rosa26*^{Grhl3 cDNA/Grhl3 cDNA} and *Grhl3*^{Cre/Cre};*Rosa26*^{Grhl3 cDNA/Grhl3 cDNA} mice displayed large scale of alopecia in the dorsal region (N = 4). (B) Hematoxylin and eosin staining of adult wild-type, *Grhl3*^{Cre/+};*Rosa26*^{Grhl3 cDNA/Grhl3 cDNA} and *Grhl3*^{Cre/Cre};*Rosa26*^{Grhl3 cDNA/Grhl3 cDNA} hair follicles (N = 4). (C) Histological and immunostaining analysis of wild-type, *Grhl3*^{Cre/+};*Rosa26*^{Grhl3 cDNA/Grhl3 cDNA} and *Grhl3*^{Cre/Cre};*Rosa26*^{Grhl3 cDNA/Grhl3 cDNA} adult epidermis (N = 4). (D) Quantifications of PCNA- and Ki67-positive cells in wild-type, *Grhl3*^{Cre/+};*Rosa26*^{Grhl3 cDNA/Grhl3 cDNA} and *Grhl3*^{Cre/Cre};*Rosa26*^{Grhl3 cDNA/Grhl3 cDNA} adult epidermis. Arrowheads, clefts between the inner root sheath and the outer root sheath. SC, stratum corneum; SG, stratum granulosum; SP, stratum spinosum; SB, stratum basale; E, epidermis; D, dermis. Bar graph presented as a mean ± standard error of mean (SEM). A one-way ANOVA test following by a Dunnett's multiple comparison test between wild-type and other genotypes were used for data analysis. *P value <.05, ***P value <.001, ****P value <.00001

FIGURE 7 Misexpression of *Grhl3* does not compromise the expression of hair shaft anchorage genes *Dsg1a* and *Grhl1*. Q-RT-PCR on E18.5 epidermis showing the mRNA abundance of two hair shaft anchorage genes *Dsg1a* (A) and *Grhl1* (B) in wild-type and transgenic mice. Bar graph presented as a mean ± standard error of mean (SEM). A one-way ANOVA test following by a Dunnett's multiple comparison test between wild-type and other genotypes were used for data analysis. n.s., not significant
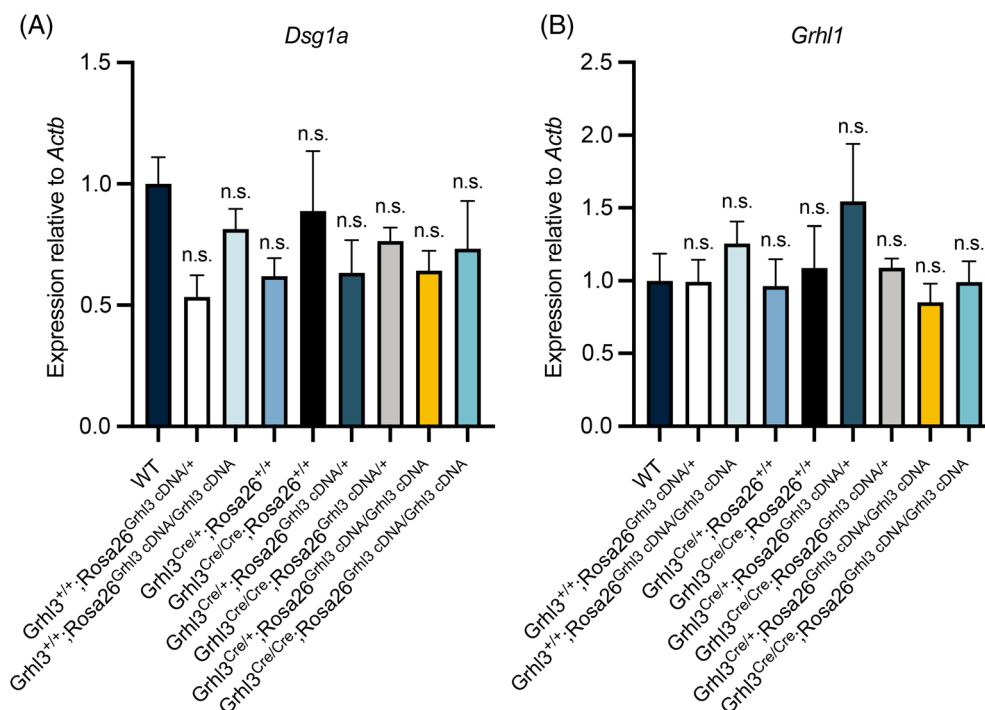
their arrangement (Figure 6C). Quantifications of the staining identified less than 35% PCNA-positive cells and around 20% Ki67-positive cells in WT epidermis, while around 60% cells were PCNA-positive and 52% were Ki67 positive in adult $Grhl3^{Cre/Cre}$;$Rosa26^{Grhl3\ cDNA/Grhl3\ cDNA}$ epidermis and the positivity percentages for PCNA and Ki67 were 43% and 35% respectively in $Grhl3^{Cre/+}$; $Rosa26^{Grhl3\ cDNA/Grhl3\ cDNA}$ adult epidermis (Figure 6D). These observations were consistent with findings in the embryonic epidermis, demonstrating that over-expression of *Grhl3* promotes hyperproliferation of basal keratinocytes in adult epidermis.

2.4 | Overexpression of *Grhl3* leads to inner ear malformation and hearing impairment

We noticed that adult mice overexpressing *Grhl3* displayed several behavioral abnormalities, including hyperactivity, poor balance, high-speed bidirectional circling, head bobbing, and head tilting. These abnormalities are collectively referred to as the Shaker-Waltzer phenotype and are typically associated with inner ear vestibular dysfunction.[30] To further investigate the correlation between *Grhl3* misexpression and the Shaker-Waltzer phenotype, we quantified the circling behaviors of adult transgenic mice. $Grhl3^{Cre/Cre}$;$Rosa26^{Grhl3\ cDNA/Grhl3\ cDNA}$ mice performed more than 80 rpm on average, whereas $Grhl3^{Cre/+}$;$Rosa26^{Grhl3\ cDNA/Grhl3\ cDNA}$ mice circled around 40 times

per minute (Figure 8A). In contrast, WT mice showed no circling behavior (Figure 8A). We previously showed that $Grhl3^{+/-}$;$Vangl2^{+/-}$ mice exhibited disordered orientation of stereociliary bundles on the sensory hair cells in the cochlea, due to disruption of the PCP pathway.[5] Therefore, we sought to investigate whether the Shaker-Waltzer phenotype resulted from cochlear hair cell misorientation. This was not the case, with cochlear phalloidin staining showing well-organized inner and outer hair cells on cochlear basilar membrane of transgenic newborns aged between postnatal days 1 and 7 (Figure 9A).

Given the normal stereociliary morphology, we postulated that Shaker-Waltzer phenotype may originate from structural defects of the inner ear. We therefore visualized this structure using micro-computed tomography (μCT) scanning. The μCT analysis was performed with the vestibular labyrinth and cochlea enclosed by the auditory bulla to minimize structural damage, followed by a 3D reconstruction to provide clearer images of the internal structure. The WT inner ear exhibited structural integrity of lateral, posterior, and anterior semi-circular canals, ampullae, and cochlea. In contrast, the posterior and anterior semi-circular canals of the $Grhl3^{Cre/Cre}$; $Rosa26^{Grhl3\ cDNA/+}$ inner ear were completely truncated, and the lateral semi-circular canals were grossly enlarged compared to WT (Figure 8B). The ampullae in these mice were also enlarged or absent, and the cochleae were strikingly larger in size compared to WT but with a relatively intact structurally (Figure 8B). The $Grhl3^{Cre/Cre}$;
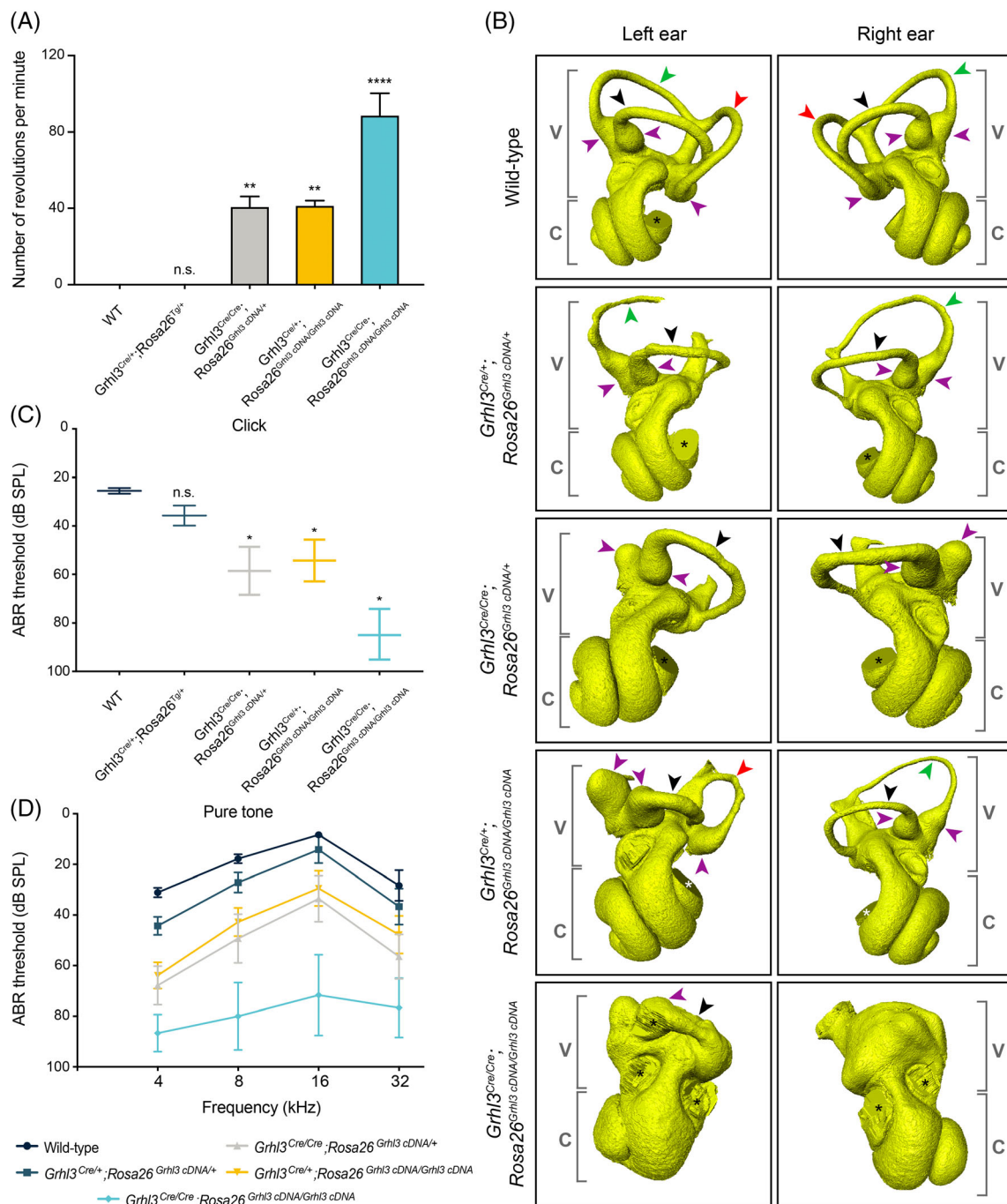
FIGURE 8   Inner ear malformation and hearing impairment in *Grhl3* transgenic mice. (A) Quantification of the number of times that transgenic mice circled per minute (N = 3-4 mice per genotype). (B) 3D reconstructions of the inner ear X-ray micro-computed tomography scanning. (C) Average ABR thresholds of wild-type (N = 10), *Grhl3*^Cre/+^;*Rosa26*^Grhl3 cDNA/+^ (N = 7), *Grhl3*^Cre/Cre^;*Rosa26*^Grhl3 cDNA/+^ (N = 7), *Grhl3*^Cre/+^;*Rosa26*^Grhl3 cDNA/Grhl3 cDNA^ (N = 7) and *Grhl3*^Cre/Cre^;*Rosa26*^Grhl3 cDNA/Grhl3 cDNA^ (N = 3) mice when respond to a click containing mixed frequency noise. (D) Average ABR thresholds of wild-type (N = 9), *Grhl3*^Cre/+^;*Rosa26*^Grhl3 cDNA/+^ (N = 7), *Grhl3*^Cre/Cre^;*Rosa26*^Grhl3 cDNA/+^ (N = 7), *Grhl3*^Cre/+^;*Rosa26*^Grhl3 cDNA/Grhl3 cDNA^ (N = 9) and *Grhl3*^Cre/Cre^;*Rosa26*^Grhl3 cDNA/Grhl3 cDNA^ (N = 3) mice when respond to pure tone stimuli at 4, 8, 16, and 32 kHz. Black arrowheads, lateral semi-circular canal; green arrowheads, posterior semi-circular canal; red arrowheads, anterior semi-circular canal; purple arrowheads, ampullae; asterisks, artifacts of the scanning and reconstruction. V, vestibular apparatus; C, cochlea. Bar graph and scatter plots presented as a mean ± standard error of mean (SEM). A one-way ANOVA test following by a Dunnett's multiple comparison test between wild-type and other genotypes were used for data analysis. *P value <.05, **P value <.01, ****P value <.00001. n.s., not significant

FIGURE 9 Misexpression of *Grhl3* does not impair the orientation of cochlea hair cell stereocilia and loss of *Grhl3* expression does not cause inner ear malformation. (A) Phalloidin staining of cochlea hair cells from the inner ear of postnatal wild-type and transgenic mice. N = 3. Scale bar = 10 μm. (B) Skeletal preparations of heads from E18.5 wild-type and *Grhl3^{Cre/Cre}*;*Rosa26^{+/+}* embryos. N = 4. C, cochlea. Black arrowheads, lateral semi-circular canal; green arrowheads, posterior semi-circular canal; red arrowheads, anterior semi-circular canal
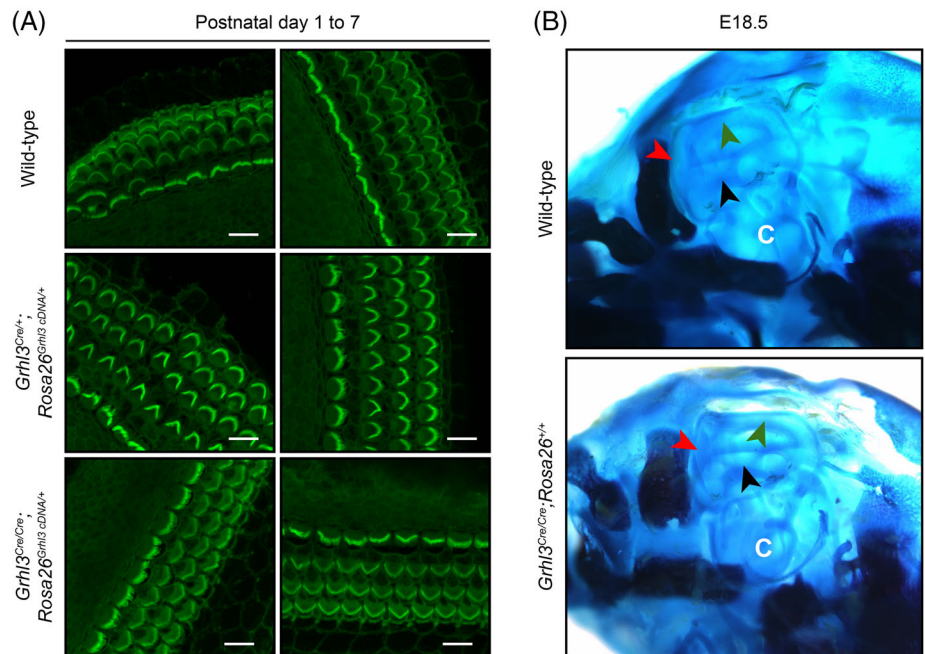
Rosa26^{Grhl3 cDNA/Grhl3 cDNA} inner ear was totally deformed, with bulbous cochleae lacking structural definition, and mostly absent or truncated semi-circular canals and ampullae (Figure 8B). As *Grhl3^{Cre/Cre}*; *Rosa26^{+/+}* embryos died soon after birth, we examined the E18.5 skeletal preparations of the temporal bones. The *Grhl3^{Cre/Cre}*;*Rosa26^{+/+}* inner ear showed normal morphological appearance that resembled the WT controls (Figure 9B). These observations indicate that *Grhl3* misexpression compromises inner ear morphogenesis and leads to Shaker-Waltzer phenotype.

To identify whether inner ear malformation leads to hearing impairment, we performed an auditory brainstem response (ABR) test to assess the hearing capacity of transgenic mice. In this test, the ABR threshold, which is the quietest sound that elicits an ABR, is similar to the hearing threshold.[31] Commensurate with the inner ear malformations, the ABR test revealed significant hearing impairment in *Grhl3*-overexpressing mice compared to WT controls (Figure 8C,D), with the average ABR threshold of WT mice at 26 dB sound pressure level (dB SPL), compared to 59 dB SPL in *Grhl3^{Cre/Cre}*;*Rosa26^{Grhl3 cDNA/Grhl3 cDNA}* mice and 85 dB SPL in *Grhl3^{Cre/Cre}*;*Rosa26^{Grhl3 cDNA/Grhl3 cDNA}* mice when responding to mixed frequency noise. At the single-frequency level, hearing impairment was most significant in *Grhl3^{Cre/Cre}*;*Rosa26^{Grhl3 cDNA/Grhl3 cDNA}* mice when responding to 4, 8, 16, and 32 kHz pure tone stimuli, but *Grhl3^{Cre/+}*;*Rosa26^{Grhl3 cDNA/Grhl3 cDNA}* mice also showed a severe hearing impairment (Figure 8D). Moreover, the overall average ABR threshold across different genotypes also displayed a stepwise increase with a threshold shift at around 6-10 dB SPL in *Grhl3^{Cre/+}*;

Rosa26^{Grhl3 cDNA/+} mice, 20-30 dB SPL in *Grhl3^{Cre/+}*; *Rosa26^{Grhl3 cDNA/Grhl3 cDNA}* mice, 25-35 dB SPL in *Grhl3^{Cre/Cre}*;*Rosa26^{Grhl3 cDNA/+}* mice, and at 48-64 dB SPL in *Grhl3^{Cre/Cre}*;*Rosa26^{Grhl3 cDNA/Grhl3 cDNA}* mice (Figure 8D). Importantly, the shape and width of click-evoked ABR peaks were normal in all tested mice (Figure 10), indicating that hearing impairment in transgenic mice resulted from inner ear structural defects rather than abnormality of the vestibulocochlear nerve or brainstem.

3 | DISCUSSION

In this study, we have for the first time successfully overexpressed *Grhl3* in adult mice, allowing us to uncover previously unsuspected developmental events that are dependent on stringent regulation of GRHL3. We achieved this using a *Grhl3*-null allele (*Grhl3^{Cre}*) to induce expression of a *Grhl3* transgene inserted into the murine *Rosa26* locus. Mice homozygous for the null allele (*Grhl3^{Cre/Cre}*) and lacking transgene expression exhibited the classic defects described in the original *Grhl3* constitutive knockout,[8] of neural tube defects, short longitudinal body axis, failure of the skin barrier to form and peri-natal lethality. These defects were completely rescued in mice carrying two copies of the *Rosa26*-based transgene, with the animals surviving to adulthood. However, multiple novel phenotypic abnormalities were observed as a consequence of dysregulated *Grhl3* expression, with digit defects, impaired epidermal homeostasis with alopecia, the Shaker-Waltzer phenotype, hearing impairment, and inner ear malformations all evident.
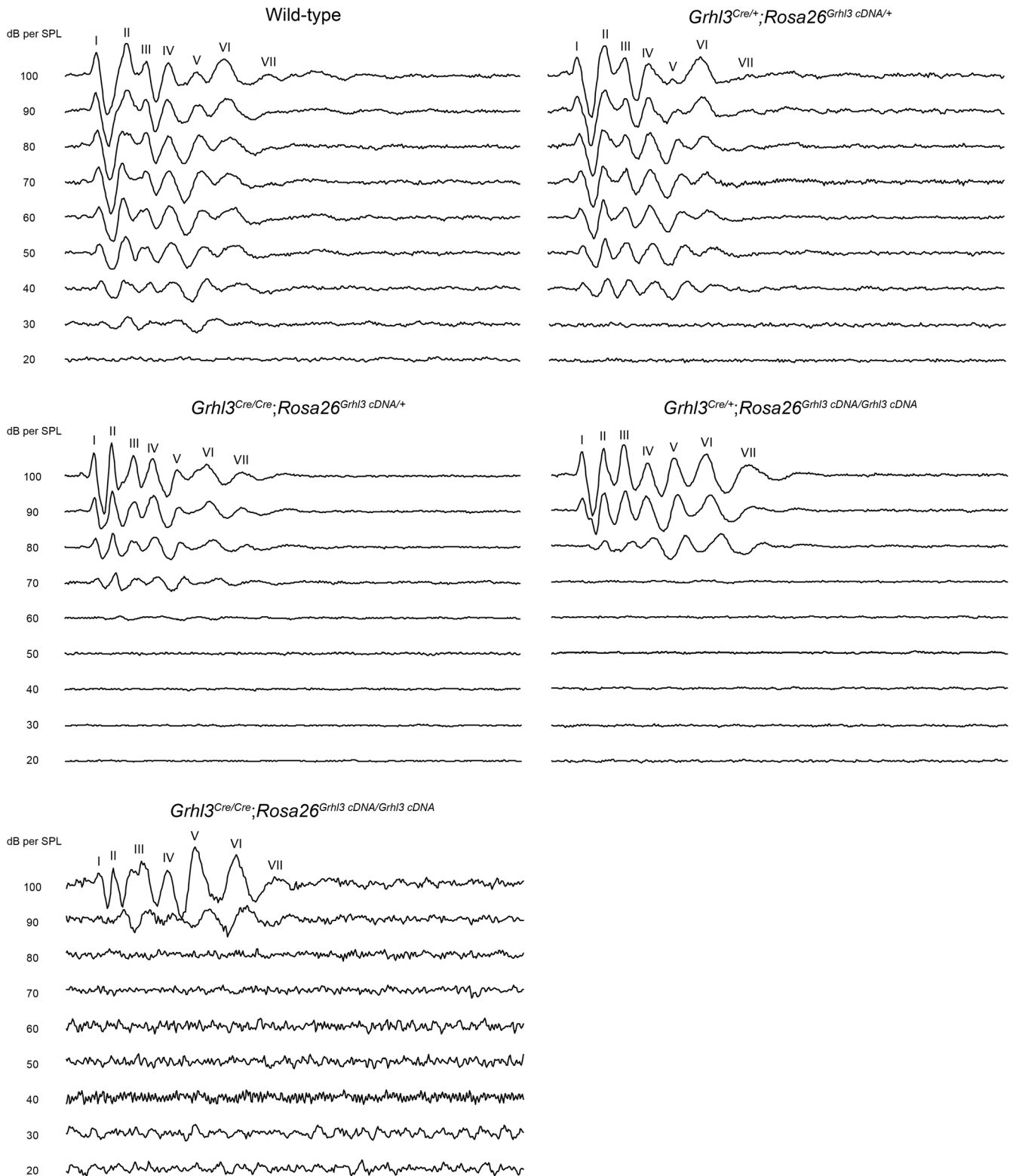
FIGURE 10 Misexpression of *Grhl3*-induced hearing impairment is not a neurological condition. Representative click-evoked ABR waveforms from wild-type (N = 10), *Grhl3*$^{Cre/+}$;*Rosa26*$^{Grhl3\ cDNA/+}$ (N = 7), *Grhl3*$^{Cre/Cre}$;*Rosa26*$^{Grhl3\ cDNA/+}$ (N = 7), *Grhl3*$^{Cre/+}$; *Rosa26*$^{Grhl3\ cDNA/Grhl3\ cDNA}$ (N = 7) and *Grhl3*$^{Cre/Cre}$;*Rosa26*$^{Grhl3\ cDNA/Grhl3\ cDNA}$ (N = 3) adult mice. I–VII represent the presences of ABR peaks, with each peak corresponds to one action potential as signal transmits through the vestibulocochlear nerve and the brainstem

De Castro et al[21] reported the first successful attempt of overexpressing *Grhl3* in late-stage mouse embryos, utilizing the hypomorphic *curly tail* strain to generate the line.[9] *Grhl3* expression was driven by a bacterial artificial chromosome (BAC), encompassing the endogenous *Grhl3* locus. A ~1.5 to 2-fold increase in total *Grhl3* mRNA expression above WT levels was documented in the caudal region of E9.5 and E10.5 embryos and a less than 1.2-fold increase in the epidermis of E18.5 embryos that were double homozygotes for $Grhl3^{ct}$ allele and the BAC transgene ($Grhl3^{ct/ct;TgGrhl3/TgGrhl3}$). Interestingly, 67% of these embryos displayed NTDs, a phenotype we never observed in our transgenic embryos, despite comparable levels of *Grhl3* overexpression. None of the De Castro et al.[21] embryos displayed digit defects or abnormal epidermal morphology, and phenotypes in adult mice were not reported. The phenotypic discrepancies between the two lines, particularly the NTDs, cannot be attributed to differences in the initial timing, location, or magnitude of expression of *Grhl3*. Both lines restricted expression to tissues that usually express *Grhl3* at the appropriate developmental time-point; De Castro et al[21] through use of the endogenous locus in a BAC, and our line via *Cre* expression from the endogenous locus activating the transgene. However, several other differences may underlie the phenotypic discrepancies. First, *Grhl3* once overexpressed in our line would remain so, as the *Rosa26* locus lacks any endogenous regulatory elements that are retained in the BAC and may influence *Grhl3* expression. Also, the overexpression line described by De Castro et al[21] had the BAC inserted into chromosome 18; therefore, it is likely that the endogenous *Grhl3* locus in the BAC does not have access to necessary mechanisms for long-range control of expression like long-range enhancers or distal *cis*-regulatory elements, may also resulting in altered *Grhl3* expression compared to the endogenous gene located on chromosome 4. Second, and in our view more likely, *Grhl3* mRNA and protein is derived from a cDNA construct in our transgene, whereas it is derived from the endogenous locus in the BAC. Several studies have highlighted the importance of intronic RNA for *GRHL3* regulation,[32-34] particularly in the context of epidermal differentiation.[32] Lack of intronic elements in our transgenic embryos may lead to further dysregulation of *Grhl3* expression. This implies that correct regulation of *Grhl3* expression is crucial for embryonic development of multiple systems. Similarly, overexpression of *Grhl3* has previously been shown to induce different developmental consequences in different models.[21,22]

A surprising finding in our model, was the underrepresentation of embryos homozygous for the transgene (irrespective of the presence or absence of a *Cre* allele) at both E14.5 and E18.5, suggesting that "leaky" expression of the transgene in very early embryogenesis had dire developmental consequences highly likely happened before or around implantation, especially in the presence of the endogenous *Grhl3* expression. This is supported by the lack of resorbed $Grhl3^{+/+};Rosa26^{Grhl3\ cDNA/Grhl3\ cDNA}$ embryo at E18.5. This finding is in keeping with the previous reports on the $Actb^{Cre};CAG^{LSL-Grhl3}$ mouse line, which displayed early lethality at E5.5.[23] We postulate that this may result from random transmission of Cre recombinase from the sperm to the oocyte where the unexpected deletion of the upstream *loxP-STOP-loxP* sequence of the transgene occurred even if the consequential embryos are *Cre* "negative" genetically,[35] or the inheritance of *delta* allele (activated transgene allele) by the offspring due to germline recombination occurred during gametogenesis in male $Grhl3^{Cre/+};Rosa26^{Grhl3\ cDNA/+}$ mice,[36] leading to certain level of *Grhl3* expression that is incompatible with early embryonic survival. Therefore, surviving homozygous transgenic mice presumably had faithful transgene expression, that commenced only after *Grhl3-Cre* was activated at E8.5. This is consistent with our PCR and Q-RT-PCR analyses showing no deletion of the *loxP-STOP-loxP* cassette, or *Grhl3* transgene expression, in E18.5 $Grhl3^{+/+};Rosa26^{Grhl3\ cDNA/Grhl3\ cDNA}$ embryos.

In $Grhl3^{Cre/Cre};Rosa26^{Grhl3\ cDNA/Grhl3\ cDNA}$ embryos, transgene-mediated expression of *Grhl3* fully rescued the epidermal barrier defect and largely normalized keratinocyte terminal differentiation in both embryos and adult mice. Surprisingly, it did not correct basal cell hyperproliferation and expansion. Previous studies have shown that diverse mechanisms centered on reducing *Grhl3* RNA levels are critical for maintaining low levels of GRHL3 protein expression in epidermal stem cells, thereby preventing differentiation.[32,34] Consistent with this, constitutive *Grhl3*-knockout mice display failed epidermal differentiation associated with expansion of a proliferative stem cell pool.[11,13,15] Therefore, the persistence of a hyperproliferative and expanded basal layer, despite normal differentiation shown here, would suggest that it is not simply the level of *Grhl3* mRNA that is important for epidermal stem cell behavior. In keeping with this, hyperproliferation in the $Grhl3^{Cre/Cre};Rosa26^{Grhl3\ cDNA/+}$ epidermis was far greater than in $Grhl3^{Cre/+};Rosa26^{Grhl3\ cDNA/+}$ epidermis, despite both lines having comparable total *Grhl3* mRNA levels. Similarly, $Grhl3^{Cre/+};Rosa26^{Grhl3\ cDNA/Grhl3\ cDNA}$ mice exhibited less basal cell proliferation than $Grhl3^{Cre/Cre};Rosa26^{Grhl3\ cDNA/Grhl3\ cDNA}$ mice despite slightly higher levels of total *Grhl3* expression. These findings suggest that either the endogenous transcript is important for stem cell homeostasis or that higher levels of transgene expression are deleterious to

stem cell behavior. Interestingly, we did not see skin papilloma formation or tumorigenesis in aged transgenic mice, however, given the presence of basal hyperproliferation, we predict that these transgenic mice may have enhanced susceptibility to chemical carcinogen-induced squamous cell carcinoma like animals with *Grhl3* conditionally inactivated in their epidermal keratinocytes.[15]

Another unexpected skin phenotype, severe alopecia, was also observed as a consequence of *Grhl3* overexpression. Our previous studies in adult conditional *Grhl3*-knockout mice revealed no alopecia,[28] whereas both *Grhl3*$^{Cre/Cre}$;*Rosa26*$^{Grhl3\ cDNA/Grhl3\ cDNA}$ and *Grhl3*$^{Cre/+}$; *Rosa26*$^{Grhl3\ cDNA/Grhl3\ cDNA}$ mice displayed dorsal hair loss that mimicked the grooming alopecia phenotype we had previously observed in constitutive *Grhl1*-knockout mice.[29] In that line, alopecia was due to poor hair anchorage as a result of detachment of the IRS from the ORS, due to loss of expression of the GRHL1 target gene, *Dsg1a*. Neither *Grhl1* nor *Dsg1a* levels were altered in the *Grhl3* over-expressing lines compared to WT, suggesting that the hair anchorage phenotype may be due to perturbed expression of other Desmoglein genes.[37,38] As this phenotype was more severe in mice with higher levels of transgene expression, and given the complete absence of a comparable phenotype in adult *Grhl3* conditional knockout mice,[28] it is unlikely that the presence of the endogenous transcript exerts any influence on hair anchorage.

Although GRHL1 deficiency causes inner ear malformation in zebrafish, and *GRHL2* has been identified as an autosomal-dominant deafness gene in humans, *Grhl3* has not previously been linked to inner ear structural defects or hearing impairment.[39-41] Our previous research had identified a key role for *Grhl3* with *Vangl2* in planar cell polarity mediated orientation of cochlear hair cell stereocilia.[5] Here, we found that misexpression of *Grhl3* had no impact on cochlear hair cell orientation, but did result in severe bony labyrinth dysmorphogenesis. Normally, the semi-circular canals provide sensory input for rotary movement, with the end of each canal extending into an ampulla in which hair cells excite the afferent fiber of the vestibular nerve upon head and body movement.[42,43] The lateral and superior canals detect the movement in vertical axis and lateral axis, respectively, and structural defects result in head tilting in mice. The posterior canal detects movement in left–right axis and defects result in circling behavior in mice.[42,43] The transgenic mice displayed vestibular disturbance, and a Shaker-Waltzer phenotype that mirrored the degree of severity of the ampulla and semi-circular canal malformation. The ABR test also revealed a positive correlation between hearing impairment and the severity of inner ear structural defects. Interestingly, severity was again linked to the levels of expression of the transgene rather than total *Grhl3* mRNA levels, with *Grhl3*$^{Cre/Cre}$; *Rosa26*$^{Grhl3\ cDNA/+}$ mice more severely afflicted than *Grhl3*$^{Cre/+}$;*Rosa26*$^{Grhl3\ cDNA/+}$ animals. Given that the *Grhl3*$^{Cre/Cre}$;*Rosa26*$^{+/+}$ inner ear showed normal morphological appearance, it appears that the levels of expression of the transgene rather than loss of the endogenous transcript is detrimental to inner ear development.

A recent study identified that intron 1 of the nascent human *GRHL3* RNA provides binding sites for the cleavage and polyadenylation specificity factor (CPSF) complex and HNRNPA3. This suppresses exonic splicing and promotes intronic polyadenylation, lowering GRHL3 expression and preventing the premature differentiation of primary human keratinocytes.[32] In humans, four alternatively spliced isoforms of *GRHL3* have been characterized[2,18,44] Although no murine *Grhl3* splice isoforms have been discovered to date, it is likely that *Grhl3* alternative splicing is conserved in mouse to generate transcript variants.[45] Early in embryonic development, the precursor of the inner ear, the otic placode, is derived from the preplacodal region (PPR), located in the territory of the neural plate border.[7,46] Notably, expression of the PPR marker, *Six1*, overlaps with *Grhl3* spatiotemporally in mouse embryos, and a recent study also showed the expression of *GRHL3* in the developing otic placode of chicken embryos.[6,47,48] We propose that due to the unregulatable *Grhl3* misexpression, the cDNA-based *Grhl3* transgene may induce abnormal differentiation of the PPR and impair the development of the otic placode and consequently, lead to inner ear defects and hearing impairment. This may indicate that a specific unidentified murine *Grhl3* mRNA isoform allows this process to occur, and overexpression of the incorrect, unregulatable splice isoform from the transgene perturbs inner ear development.

In conclusion, our study has highlighted that stringent regulation of *Grhl3* expression is an absolute requirement for numerous developmental processes. In particular, epidermal differentiation and hair anchorage, digit formation, and formation of the cochlea and vestibular apparatus are affected. In addition, it has raised the concept that not only are the levels of the transcription factor important but also that isoform-specific roles may govern different morphogenetic events.

4 | EXPERIMENTAL PROCEDURES

4.1 | Mice

To misexpress *Grhl3*, a *Flag-Grhl3* transgene preceded by a floxed transcriptional stop sequence (*Rosa26*$^{Grhl3\ cDNA}$)

was activated by *Grhl3* knock-in-*Cre* (*Grhl3^Cre^*). This generated a mouse (*Grhl3^Cre^*;*Rosa26^Grhl3 cDNA^*) that express FLAG-GRHL3 in place of endogenous GRHL3. The *Rosa26^Grhl3 cDNA^* mouse line was generated as described previously.[24] Briefly, a *Grhl3* cDNA-containing pENTR1A construct and a pRMCE DV1 destination vector were amalgamated into a single targeting vector through Gateway LR Clonase II (Thermo Fisher Scientific)-mediated in vitro recombination. The mouse *Grhl3* cDNA was generated as previously described.[8] The targeting vector was then introduced into the recombinase-mediated cassette exchange (RMCE)-compatible murine G4 ROSALUC embryonic stem cells (ESCs) by electroporation. Insertion into the *Rosa26* locus occurred through a FLPe-mediated RMCE. Positive clones were selected based upon 5′ PCR using a combination of external (forward 5′-AAA GCT CTG AGT TGT TAT-3′) and internal (reverse 5′-GCG GCC TCGACT CTA CGA TA-3′) primers at the site of 5′ integration and on restored neomycin resistance. Positive ESC clones were aggregated with CD1 diploid host embryos and strong chimeras bred for germline transmission of the *Rosa26^Grhl3 cDNA^* targeted allele.[49] *Grhl3^Cre^* mice[25] were crossed with *Rosa26^Grhl3 cDNA/Grhl3 cDNA^* mice and *Grhl3^Cre/+^*;*Rosa26^Grhl3 cDNA/+^* offspring were intercrossed through timed mating overnight. Deletion of the floxed transcriptional stop sequence was confirmed by PCR using genomic DNA isolated from E18.5 epidermis with the following primers: *floxed* forward (5′-GAG GAC AAA CTC TTC GCG GT-3′), *floxed* reverse (5′-CAG AGG CTG CTG ATC TCG TT-3′), *delta* reverse (5′-TAT CCG CTT CTC CTT GGG AC-3′). The PCR product size of the *floxed* allele is 631 bp and of the *delta* allele is 492 bp. The generation and genotyping of *Grhl3^−/−^* mice have been previously described.[8] The *Grhl3^Cre^*;*Rosa26^Grhl3 cDNA^* line was maintained under a mixed background and the *Grhl3*-null line was maintained on a C57BL/6 background. The gestational age of embryos was identified as E0.5 at midday on the day of detection of a vaginal plug. All the animal experiments were approved by the Alfred Research Alliance Animal Ethics Committee with project number E/1800/2018/M, E/1900/2019/M, E/8285/2022/M, and E/8286/2022/M. Research was conducted in the accordance of the Australian Code for the Care and Use of Animals for Scientific Purposes and the Australian Code for the Responsible Conduct of Research.

4.2 | Genotyping of mice

Mice were genotyped using genomic DNA isolated from tails biopsies or yolk sacs by PCR. The *Grhl3* knock-in-*Cre* allele was genotyped using the following primers: *Grhl3KI-Cre* forward (5′-CAC CCC CTC AGC TAA GAA GGA A-3′), *Grhl3KI-Cre* WT reverse (5′-CCC TTT GGC AAG AGG AGA GAA A-3′) and *Grhl3KI-Cre* KI reverse (5′-TCC CTG AAC ATG TCC ATC AGG T-3′). The PCR product size of the WT allele is 702 bp and of the *Cre* allele is 420 bp. The *Grhl3* transgene at the *Rosa26* locus was genotyped using the following primers: *Rosa26* 5′ (5′-AAA GTC GCT CTG AGT TGT TAT-3′), *Rosa26* WT 3′ (5′-GGA GCG GGA GAA ATG GAT ATG-3′) and *Rosa26* MUT 3′ (5′-GCG AAG AGT TTG TCC TCA ACC-3′). The PCR product size of the WT allele is 600 bp and of the *Grhl3* transgene on *Rosa26* allele is 300 bp.

4.3 | Skin barrier assay and skeletal preparation

For skin barrier assay, embryos were fixed in methanol on a roller mixer for 5 minutes and then washed in PBS twice for 5 minutes. Fixed embryos were incubated in 0.1% (w/v) toluidine blue for 5 minutes, then washed, imaged and stored in PBS at 4°C. Skeletal preparations were performed as previously described.[50] Images of embryos and skeletal preparation were obtained using Nikon SMZ1500 stereomicroscope with AxioVision software (Zeiss).

4.4 | Histology and IHC

For histological analysis, skin samples were fixed in 4% (w/v) PFA for at least 24 hours at room temperature (RT). Samples were then processed using a Leica ASP300S and embedded into paraffin. Samples were sectioned in a transverse orientation at 5 μm thickness and collected onto SuperFrost plus slides (Thermo Fisher Scientific). H&E staining was performed using standard methods. IHC was performed as per standard protocols using the DAB Peroxidase Substrate Kit (Vector Laboratories). Images of sections were obtained using a Nikon ECLIPSE Ci-L upright microscope with NIS-Elements D software, then analyzed and quantified using ImageJ software and GraphPad Prism 8. Antibodies used for IHC were anti-Keratin 1 (Covance, PRB-149P-100; 1:500, 45 minutes, RT), anti-Filaggrin (Covance, PRB-417P-100; 1:1000, 45 minutes, RT), anti-Loricrin (Covance, PRB-145P-100; 1:500, overnight, 4°C), anti-Involucrin (Covance, PRB-140C; 1:750, 10 minutes, RT), anti-Keratin 5 (Covance, PRB-160P; 1:500, 45 minutes, RT), anti-Keratin 14 (Covance, PRB-155P; 1:1000, 45 minutes, RT), anti-Keratin 6 (Covance, PRB-169P-100; 1:500, 45 minutes, RT), anti-PCNA (CST, 2586, 1:2000, 30 minutes, RT), anti-Ki67 (Abcam, ab16667, 1:100, overnight, 4°C) and goat anti-rabbit secondary antibody

(Vector Laboratories, ZB0318; 1:200, 30 minutes, RT). For IHC with anti-PCNA antibody, the Mouse-on-Mouse immunodetection kit (Vector Laboratories) was used as per the manufacturer's instructions.

4.5 | Phalloidin staining and confocal microscopy

To access hair cells, first, bony labyrinth was dissected from mice at the age of postnatal 1-6 days. Then, cochlea was opened and the spiral ligament and the attached organ of Corti were separated from cochleae. The organ of Corti was separated from the spiral ligament, and the hair cell-containing sensory epithelia were separated from the spiral limbus of organ of Corti and fixed in 4% (w/v) PFA at 4°C for at least 24 hours. Hair cell Phalloidin staining was performed as previously described.[5] Samples were imaged using a Nikon Eclipse Ti inverted A1R confocal microscope through a CFI Apochromat TIRF ×60 Oil objective. A total 15-30 images spaced 0.5 μm apart were collected by NIS-Elements Advanced Research software. The images were then analyzed by ImageJ software.

4.6 | Mice behavioral examination and auditory brainstem response test

An individual mouse was placed in a single cage. Physical activities within 1 minute were recorded using a Canon EOS 60D camera. Circling behavior was quantified by manual counting and analyzed using GraphPad Prism 8. For auditory brainstem response (ABR) test, mice were anaesthetized through intraperitoneal injection of anesthetic mixture (100 mg/kg ketamine, 50 mg/kg xylazine, and 30 mg/kg acepromazine). Mice eyes were covered by lubricating eye ointment (Poly Visc, Alcon) to avoid desiccation and body temperature was maintained with a 37°C heating pad. Anesthesia was confirmed by the absence of the pedal reflex. ABR test was performed using an evoked potential workstation (Tucker Davis Technologies). Briefly, an anaesthetized mouse was placed inside a Faraday cage, with a free-field magnetic speaker installed 10 cm from the left pinna. The Faraday cage was contained by a sound attenuation chamber. A 100 μs click with a frequency between 0 and 50 kHz and a set of 3 ms pure tone stimuli at 4, 8, 16, and 32 kHz were delivered with maximum intensities of 100 dB SPL. ABRs were detected using three subdermal electrodes (Rochester Electro-Medical): the positive electrode was deposited at the vertex of the skull; the negative electrode was positioned in the left cheek and the

ground electrode was placed at the hind left leg. Through the positive electrode, the auditory evoked potential can be extracted from the neural electrical activity and transformed into waveforms. BioSig software (Tucker Davis Technologies) was used to determine the ABR threshold by averaging collected ABRs over 512 repetitions of each stimulus. The lowest consistent ABR-evoking intensity stimulus was identified as the threshold.

4.7 | X-ray microcomputed tomography

Adult mice were sacrificed and the inner ear containing auditory bulla was dissected from the petrous part of the temporal bone as previously described.[51] Samples were fixed in 10% (v/v) neutral buffered formalin (NBF) at RT. X-ray μCT scanning was performed using an Xradia MicroXCT-200 (Carl Zeiss X-ray Microscopy) as described.[52] Three-dimensional (3D) reconstructed images were obtained and segmented using Avizo-6.2 software (Mercury Computer Systems). 3D modeling and following analyses were performed in blinded to genotypes.

4.8 | Reverse transcription and quantitative polymerase chain reaction

Mice dorsal skin samples were harvested, and snap froze in liquid nitrogen. Epidermis was separated from the skin by incubating with 1 mg/mL dispase in PBS at 4°C overnight. Epidermis was then homogenized in TRIsure (Bioline) and RNA was isolated according to the manufacturer's instructions. RNA was then treated by a TURBO DNA-free kit (Invitrogen) to remove genomic DNA and reverse transcribed using a Transcriptor First Strand cDNA Synthesis Kit (Roche). Quantitative reverse transcription PCR (Q-RT-PCR) was performed using GoTaq qPCR master mix (Promega) on a LightCycler 480 Instrument (Roche). Relative expression values were generated using the ΔΔCT method by standardizing genes of interest to *Actb* and analyzed using GraphPad Prism 8. Oligonucleotide primers used for Q-RT-PCR were *Grhl3* endogenous and transgene forward (5′-CGA GGC CTG GAA GAC ATA CC-3′), *Grhl3* endogenous and transgene reverse (5′-CTC AGA GCA GCC ACA CTC TC-3′), *Grhl3* endogenous forward (5′-AGC CAA CCA GAG ACG GAT C-3′), *Grhl3* endogenous reverse (5′-AGG CCT CGT CCT CAT TAC TG-3′), *Grhl3* transgene forward (5′-ACA AGG ACG ACG ATG ACA AG-3′), *Grhl3* transgene reverse (5′-CCG TTG ACT CTC ATC ATG GC-3′), *Tgm1* forward (5′-CTC CTT CTG GGC TCG TTG TT-3′), *Tgm1* reverse (5′-ATT TAC ACC ACT GCC

CCG AG-3′), *Grhl1* forward (5′-GCG CGA TGA CAC AGG AGT A-3′), *Grhl1* reverse (5′-GGA ACG ACT TCC AGG CTT CA-3′), *Dsg1a* forward (5′-GGG ATA ACC ACC ATC TGT GT-3′), *Dsg1a* reverse (5′-CCT CCC AGA TCT TGC ATT TC-3′), *Actb* forward (5′-GAT ATC GCT GCG CTG GTC GTC-3′), and *Actb* reverse (5′-CAG CTC ATT GTA GAA GGT GTG G-3′).

4.9 | Western blotting

Mice dorsal epidermis samples were lysed in radioimmunoprecipitation assay (RIPA) buffer containing a protease inhibitor cocktail and DMSF at 4°C for 2 hours. Equal amounts of denatured protein from each sample were separated on a NuPAGE 12% Bis-Tris Gel (Invitrogen) and transferred onto an Amersham Hybond P 0.45 PVDF blotting membrane (GE Healthcare). For blocking and antibody dilution, 5% skim milk in $1\times$ TBST ($1\times$ Tris-buffered saline with 0.1% Tween 20) was used. Antibodies used for western blotting were anti-GRHL3 (targeting amino acid 195-211 as previously described,[23] 1:1000, overnight, 4°C), anti-beta-Actin (CST, 5125 S; 1:1000, overnight, 4°C), anti-GFP (BioVision, 3999-100; 1:5000, overnight, 4°C) and ECL peroxidase labeled anti-rabbit secondary antibody (GE Healthcare, NA934VS; 1:5000, 1.5 hours, RT). The protein membrane was developed with the SignalFire Elite ECL Reagent (CST) and visualized using the ChemiDoc imaging system (Bio-Rad).

4.10 | Statistical analysis

A one sample χ^2 test was used to compare the expected and observed numbers of E18.5 embryos, *P* values were determined with 1° of freedom. Relative expression of genes, % of PCNA-positive cells in epidermis, number of mice revolutions per minute and average ABR thresholds were compared between wild-type and other genotypes using one-way ANOVA tests following by Dunnett's multiple comparison tests with a GraphPad Prism 8 software. When comparing the total *Grhl3* mRNA abundance between wild-type and *Grhl3$^{Cre/Cre}$;Rosa26$^{Grhl3\ cDNA/Grhl3\ cDNA}$* animals in Figure 2A, an additional Mann-Whitney test was used with a GraphPad Prism 8 software.

AUTHOR CONTRIBUTIONS
Zihao Deng: Conceptualization (supporting); data curation (lead); formal analysis (equal); investigation (lead); methodology (supporting); project administration (lead); validation (supporting); visualization (lead); writing – original draft (lead). **Tariq Butt:** Data curation (supporting); formal analysis (supporting); investigation (supporting); methodology (supporting); project administration (supporting); validation (supporting). **Benedicta D. Arhatari:** Data curation (supporting); formal analysis (supporting); investigation (supporting); methodology (supporting). **Charbel Darido:** Conceptualization (supporting); investigation (supporting); methodology (supporting). **Alana Auden:** Formal analysis (supporting); investigation (supporting); methodology (supporting). **Dijina Swaroop:** Formal analysis (supporting); investigation (supporting); methodology (supporting). **Darren D. Partridge:** Formal analysis (supporting); investigation (supporting); methodology (supporting). **Katharina Haigh:** Formal analysis (supporting); investigation (supporting); methodology (supporting). **Thao Nguyen:** Formal analysis (supporting); investigation (supporting); methodology (supporting). **Jody J. Haigh:** Formal analysis (supporting); investigation (supporting); methodology (supporting). **Marina R. Carpinelli:** Conceptualization (lead); data curation (supporting); formal analysis (supporting); investigation (supporting); methodology (supporting); project administration (equal); supervision (equal). **Stephen M. Jane:** Conceptualization (lead); data curation (equal); formal analysis (equal); funding acquisition (equal); investigation (supporting); methodology (equal); project administration (lead); resources (lead); software (supporting); supervision (lead); validation (supporting); visualization (supporting); writing – original draft (supporting); writing – review and editing (lead).

facilitated by Monash University, as part of the Wiley - Monash University agreement via the Council of Australian University Librarians.

CONFLICT OF INTEREST

The authors declare no conflict of interest.

DATA AVAILABILITY STATEMENT

All data that support the findings of this study are available from the corresponding author upon reasonable request.

ORCID

Zihao Deng https://orcid.org/0000-0001-5702-6648
Marina R. Carpinelli https://orcid.org/0000-0001-5115-7831
Stephen M. Jane https://orcid.org/0000-0002-1045-0481

REFERENCES

1. Wilanowski T, Tuckfield A, Cerruti L, et al. A highly conserved novel family of mammalian developmental transcription factors related to drosophila grainyhead. *Mech Dev.* 2002;114(1–2): 37-50.
2. Ting SB, Wilanowski T, Cerruti L, Zhao LL, Cunningham JM, Jane SM. The identification and characterization of human sister-of-mammalian Grainyhead (SOM) expands the grainyhead-like family of developmental transcription factors. *Biochem J.* 2003;370(Pt 3):953-962. doi:10.1042/bj20021476
3. Kudryavtseva EI, Sugihara TM, Wang N, et al. Identification and characterization of Grainyhead-like epithelial transactivator (GET-1), a novel mammalian Grainyhead-like factor. *Dev Dyn.* 2003;226(4):604-617. doi:10.1002/dvdy.10255
4. Auden A, Caddy J, Wilanowski T, Ting SB, Cunningham JM, Jane SM. Spatial and temporal expression of the Grainyhead-like transcription factor family during murine development. *Gene Expr Patterns.* 2006;6(8):964-970. doi:10.1016/j.modgep.2006.03.011
5. Caddy J, Wilanowski T, Darido C, et al. Epidermal wound repair is regulated by the planar cell polarity signaling pathway. *Dev Cell.* 2010;19(1):138-147. doi:10.1016/j.devcel.2010.06.008
6. Kimura-Yoshida C, Mochida K, Ellwanger K, Niehrs C, Matsuo I. Fate specification of neural plate border by canonical Wnt signaling and Grhl3 is crucial for neural tube closure. *EBioMedicine.* 2015;2(6):513-527. doi:10.1016/j.ebiom.2015.04.012
7. Alsina B, Whitfield TT. Sculpting the labyrinth: morphogenesis of the developing inner ear. *Semin Cell Dev Biol.* 2017;65:47-59. doi:10.1016/j.semcdb.2016.09.015
8. Ting SB, Wilanowski T, Auden A, et al. Inositol- and folate-resistant neural tube defects in mice lacking the epithelial-specific factor Grhl-3. *Nat Med.* 2003;9(12):1513-1519. doi:10.1038/nm961
9. Gustavsson P, Greene ND, Lad D, et al. Increased expression of Grainyhead-like-3 rescues spina bifida in a folate-resistant mouse model. *Hum Mol Genet.* 2007;16(21):2640-2646. doi:10.1093/hmg/ddm221
10. Jaffe E, Niswander L. Loss of Grhl3 is correlated with altered cellular protrusions in the non-neural ectoderm during neural tube closure. *Dev Dyn.* 2021;250(5):732-744. doi:10.1002/dvdy.292
11. Ting SB, Caddy J, Hislop N, et al. A homolog of drosophila grainy head is essential for epidermal integrity in mice. *Science.* 2005;308(5720):411-413. doi:10.1126/science.1107511
12. Kashgari G, Meinecke L, Gordon W, et al. Epithelial migration and non-adhesive periderm are required for digit separation during mammalian development. *Dev Cell.* 2020;52(6):764-778. e4. doi:10.1016/j.devcel.2020.01.032
13. Ting SB, Caddy J, Wilanowski T, et al. The epidermis of grhl3-null mice displays altered lipid processing and cellular hyperproliferation. *Organogenesis.* 2005;2(2):33-35. doi:10.4161/org.2.2.2167
14. Yu Z, Lin KK, Bhandari A, et al. The Grainyhead-like epithelial transactivator get-1/Grhl3 regulates epidermal terminal differentiation and interacts functionally with LMO4. *Dev Biol.* 2006;299(1):122-136. doi:10.1016/j.ydbio.2006.07.015
15. Darido C, Georgy SR, Wilanowski T, et al. Targeting of the tumor suppressor GRHL3 by a miR-21-dependent proto-oncogenic network results in PTEN loss and tumorigenesis. *Cancer Cell.* 2011;20(5):635-648. doi:10.1016/j.ccr.2011.10.014
16. Goldie SJ, Cottle DL, Tan FH, et al. Loss of GRHL3 leads to TARC/CCL17-mediated keratinocyte proliferation in the epidermis. *Cell Death Dis.* 2018;9(11):1072. doi:10.1038/s41419-018-0901-6
17. Georgy SR, Cangkrama M, Srivastava S, et al. Identification of a novel proto-oncogenic network in head and neck squamous cell carcinoma. *J Natl Cancer Inst.* 2015;107(9):1-13. doi:10.1093/jnci/djv152
18. Peyrard-Janvid M, Leslie EJ, Kousa YA, et al. Dominant mutations in GRHL3 cause Van der Woude syndrome and disrupt oral periderm development. *Am J Hum Genet.* 2014;94(1):23-32. doi:10.1016/j.ajhg.2013.11.009
19. Lemay P, Guyot MC, Tremblay E, et al. Loss-of-function de novo mutations play an important role in severe human neural tube defects. *J Med Genet.* 2015;52(7):493-497. doi:10.1136/jmedgenet-2015-103027
20. Yang W, Xiao Y, Tian T, Jin L, Wang L, Ren A. Genetic variants in GRHL3 and risk for neural tube defects: a case-control and case-parent triad/control study. *Birth Defects Res.* 2019;111(19):1468-1478. doi:10.1002/bdr2.1556
21. De Castro SCP, Gustavsson P, Marshall AR, et al. Overexpression of Grainyhead-like 3 causes spina bifida and interacts genetically with mutant alleles of Grhl2 and Vangl2 in mice. *Hum Mol Genet.* 2018;27(24):4218-4230. doi:10.1093/hmg/ddy313
22. Miles LB, Darido C, Kaslin J, Heath JK, Jane SM, Dworkin S. Mis-expression of grainyhead-like transcription factors in zebrafish leads to defects in enveloping layer (EVL) integrity, cellular morphogenesis and axial extension. *Sci Rep.* 2017;7(1): 17607. doi:10.1038/s41598-017-17898-7
23. Kimura-Yoshida C, Mochida K, Nakaya M-a, Mizutani T, Matsuo I. Cytoplasmic localization of GRHL3 upon epidermal differentiation triggers cell shape change for epithelial morphogenesis. *Nat Commun.* 2018;9(1):4059. doi:10.1038/s41467-018-06171-8
24. Haenebalcke L, Goossens S, Naessens M, et al. Efficient ROSA26-based conditional and/or inducible transgenesis using RMCE-compatible F1 hybrid mouse embryonic stem cells. *Stem Cell Rev Rep.* 2013;9(6):774-785. doi:10.1007/s12015-013-9458-z

25. Camerer E, Barker A, Duong DN, et al. Local protease signaling contributes to neural tube closure in the mouse embryo. *Dev Cell.* 2010;18(1):25-38. doi:10.1016/j.devcel.2009.11.014

26. Silver LM. *Mouse Genetics: Concepts and Applications.* New York, USA: Oxford University Press; 1995.

27. Hardman MJ, Sisi P, Banbury DN, Byrne C. Patterned acquisition of skin barrier function during development. *Development.* 1998;125(8):1541-1552.

28. Cangkrama M, Darido C, Georgy SR, et al. Two ancient gene families are critical for maintenance of the mammalian skin barrier in postnatal life. *J Invest Dermatol.* 2016;136(7):1438-1448. doi:10.1016/j.jid.2016.02.806

29. Wilanowski T, Caddy J, Ting SB, et al. Perturbed desmosomal cadherin expression in grainy head-like 1-null mice. *EMBO J.* 2008;27(6):886-897.

30. Deol MS. Inherited diseases of the inner ear in man in the light of studies on the mouse. *J Med Genet.* 1968;5(2):137-158. doi:10.1136/jmg.5.2.137

31. Zhou X, Jen PHS, Seburn KL, Frankel WN, Zheng QY. Auditory brainstem responses in 10 inbred strains of mice. *Brain Res.* 2006;1091(1):16-26. doi:10.1016/j.brainres.2006.01.107

32. Chen X, Lloyd SM, Kweon J, Gamalong GM, Bao X. Epidermal progenitors suppress GRHL3-mediated differentiation through intronic polyadenylation promoted by CPSF-HNRNPA3 collaboration. *Nat Commun.* 2021;12(1):448. doi:10.1038/s41467-020-20674-3

33. Kikulska A, Rausch T, Krzywinska E, et al. Coordinated expression and genetic polymorphisms in Grainyhead-like genes in human non-melanoma skin cancers. *BMC Cancer.* 2018;18(1):23. doi:10.1186/s12885-017-3943-8

34. Mistry DS, Chen Y, Sen GL. Progenitor function in self-renewing human epidermis is maintained by the exosome. *Cell Stem Cell.* 2012;11(1):127-135. https://doi.org10.1016/j.stem.2012.04.022

35. Song AJ, Palmiter RD. Detecting and avoiding problems when using the Cre–lox system. *Trends Genet.* 2018;34(5):333-340. doi:10.1016/j.tig.2017.12.008

36. Spinelli V, Martin C, Dorchies E, et al. Screening strategy to generate cell specific recombination: a case report with the RIP-Cre mice. *Transgenic Res.* 2015;24(5):803-812. doi:10.1007/s11248-015-9889-1

37. Hanakawa Y, Matsuyoshi N, Stanley JR. Expression of desmoglein 1 compensates for genetic loss of desmoglein 3 in keratinocyte adhesion. *J Invest Dermatol.* 2002;119(1):27-31. doi:10.1046/j.1523-1747.2002.01780.x

38. Hanakawa Y, Li H, Lin C, Stanley JR, Cotsarelis G. Desmogleins 1 and 3 in the companion layer anchor mouse anagen hair to the follicle. *J Invest Dermatol.* 2004;123(5):817-822. doi:10.1111/j.0022-202X.2004.23479.x

39. Peters LM, Anderson DW, Griffith AJ, et al. Mutation of a transcription factor, TFCP2L3, causes progressive autosomal dominant hearing loss, DFNA28. *Hum Mol Genet.* 2002;11(23):2877-2885. doi:10.1093/hmg/11.23.2877

40. Vona B, Nanda I, Neuner C, Müller T, Haaf T. Confirmation of GRHL2 as the gene for the DFNA28 locus. *Am J Med Genet A.* 2013;161A(8):2060-2065. doi:10.1002/ajmg.a.36017

41. Liu F, Yang F, Wen D, et al. Grhl1 deficiency affects inner ear development in zebrafish. *Int J Dev Biol.* 2015;59(10–12):417-423.

42. Standring S. *Gray's Anatomy: the Anatomical Basis of Clinical Practice.* 41st ed. New York: Elsevier Limited; 2016.

43. Marieb EN, Wilhelm PB, Mallatt J. *Human Anatomy.* 8th ed. San Francisco: Pearson; 2017.

44. Mangold E, Böhmer AC, Ishorst N, et al. Sequencing the GRHL3 coding region reveals rare truncating mutations and a common susceptibility variant for nonsyndromic cleft palate. *Am J Hum Genet.* 2016;98(4):755-762. doi:10.1016/j.ajhg.2016.02.013

45. Miles LB, Dworkin S, Darido C. Alternative splicing and start sites: lessons from the Grainyhead-like family. *Dev Biol.* 2017;429(1):12-19. doi:10.1016/j.ydbio.2017.06.018

46. Saint-Jeannet J-P, Moody SA. Establishing the pre-placodal region and breaking it into placodes with distinct identities. *Dev Biol.* 2014;389(1):13-27. doi:10.1016/j.ydbio.2014.02.011

47. Sato S, Ikeda K, Shioi G, et al. Conserved expression of mouse Six1 in the pre-placodal region (PPR) and identification of an enhancer for the rostral PPR. *Dev Biol.* 2010;344(1):158-171. doi:10.1016/j.ydbio.2010.04.029

48. Williams RM, Lukoseviciute M, Sauka-Spengler T, Bronner ME. Single-cell atlas of early chick development reveals gradual segregation of neural crest lineage from the neural plate border during neurulation. *eLife.* 2022;11:e74464. doi:10.7554/Elife74464

49. Nyabi O, Naessens M, Haigh K, et al. Efficient mouse transgenesis using gateway-compatible ROSA26 locus targeting vectors and F1 hybrid ES cells. *Nucleic Acids Res.* 2009;37(7):e55. doi:10.1093/nar/gkp112

50. Carpinelli MR, de Vries ME, Auden A, et al. Inactivation of Zeb1 in GRHL2-deficient mouse embryos rescues midgestation viability and secondary palate closure. *Dis Model Mech.* 2020;13(3):1-14. doi:10.1242/dmm.042218

51. Sakamoto A, Kuroda Y, Kanzaki S, Matsuo K. Dissection of the auditory bulla in postnatal mice: isolation of the middle ear bones and histological analysis. *J Vis Exp.* 2017;119:55054. doi:10.3791/55054

52. Ogier JM, Arhatari BD, Carpinelli MR, McColl BK, Wilson MA, Burt RA. An intronic mutation in Chd7 creates a cryptic splice site, causing aberrant splicing in a mouse model of CHARGE syndrome. *Sci Rep.* 2018;8(1):5482. doi:10.1038/s41598-018-23856-8